UNIVERSITY OF THESSALY

SCHOOL OF ENGINEERING

DEPARTMENT OF MECHANICAL ENGINEERING

Postgraduate Thesis

Design and Development of a Fuel Cell System (PEM Type): Preparation and Characterization of Low Platinum and Platinum Free Electrocatalysts

By

Karampogia Efthymia

Environmental Engineer University of Patras, 2012

Supervised by

Professor Panagiotis Tsiakaras

Submitted in partial fulfillment of the

Requirements for the

Degree of Master of Science in the

Department of Mechanical Engineering of the

University of Thessaly

Volos, 2015

Approved by the Members of MSc Examination Committee:

First Examiner (Supervisor)	Dr. Tsiakaras Panagiotis Professor, Department of Mechanical Engineering, University of Thessaly
Second Examiner	Dr. Andritsos Nikolaos Professor, Department of Mechanical Engineering, University of Thessaly
Third Examiner	Dr. Papathanasiou Athanasios Associate Professor, Department of Mechanical Engineering, University of Thessaly

Acknowledgements

The preparation and the development of this dissertation were made in the Laboratory of Alternative Energy Conversion Systems at the Department of Mechanical Engineering in University of Thessaly under the requirements of the Postgraduate Diploma.

Initially, I would like to deeply thank my supervisor and Professor Panagiotis Tsiakaras who guided me and trusted me and without his help this dissertation would not be completed. Furthermore, I would like to thank Professor Papathanasiou Athanasios and Professor Nikolaos Andritsos for being the two members of my MSc committee and for their time and useful help and advice.

The completion of my dissertation has been a long journey which without the invaluable support of the Laboratory's Alternative Conversion Systems Research Group I would not have managed so well. More precisely, I would like firstly to thank, Dr. Angeliki Brouzgou and Dr. Fotini Tzormpatzoglou for the excellent collaboration we had during the experimental parts of this dissertation and for their time, effort and advice. I am also indebted to people I had the pleasure to work with, whose academic support and input and personal cheering are greatly appreciated. More precisely I would like to thank Dr. Sotiria Kontou, Dr. Stratigoula Mitri, Dr. Antonios Seretis and Mr. Konstantinos Peppas for their interventions and advices during my stay in the laboratory.

Finally, I would like to give special thanks to my parents, Nikolaos and Maria that encouraged my efforts and support me in every part of my life.

Table of Contents

List of Figures

List of Tables

Abstract

Fuel cell technology has undergone significant development in the last 15 years, spurred in part by its unique energy conversion characteristics; directly converting chemical energy to electrical energy with efficiencies almost 70%. As fuel cell technology has passed through the prototype and the pre-commercialization development stage, there is increasing interest in manufacturing and application issues. Of the six different fuel cell types pursued commercially, the Proton Exchange Membrane (PEM) fuel cell has received the greatest amount of research and development investment due to its very low operation temperature and its suitability in a variety of applications. The fuel processor converts fuels such as natural gas, methanol, gasoline or bio-ethanol into the hydrogen-rich fuel required by the fuel cell or the fuel cell stack. Fuel cells are usually classified by their electrolyte.

The perfect fuel for the productive operation of fuel cells is H_2, which exists, in high amounts in nature as the principle constituent of water and natural substances. Traditional Polymer Electrolyte Membrane Fuel Cells (PEMFC) utilizing Pt as an impetus endure irreversible harm of the electrocatalytic movement if CO (even at 100ppm) is presented with the fuel gas. Hence, the fuel processor ought to have the capacity to supply the energy component with CO free H_2 thus high multifaceted nature and precariousness portray the framework.

The first important part of the present study is the analysis on the basic principles and the classification of the fuel cells and particularly of the Proton Exchange Membrane fuel cell and its components.

The materials used upon this study are the noble metal electrodes and the use of non-platinum and low platinum electrocatalysts.

In Chapter 3 the experimental equipment is referred and analyzed in detail. The physicochemical characterization was conducted by the techniques of Transmitting Electrode Microscopy (TEM) and X-Ray Diffraction (XRD). The electrochemical characterization towards hydrogen and oxygen electrooxidation

was conducted by the Cyclic Voltammetry, Chronoamperometry and Rotating Disk methods.

An experimental investigation was made for the bimetallic electrocatalysts of Pd_xRh_y and Pd_xPt_y. The results that occurred from these experiments are featured in Chapters 4 and 5 were the physicochemical and electrochemical characterization of the Pd based anodes and cathodes are demonstrated in analysis.

Moreover, experiments with the PEM fuel cell are demonstrated in Chapter 6 of the dissertation were the results show the connection between the current density and the temperature of the fuel cell as the later rises.

Furthermore, the conclusions and the perspectives of the research made are demonstrated in Chapter 7 of the dissertation as a conclusive part.

Περίληψη

Η τεχνολογία κυψελών καυσίμου έχει επισέλθει σε σημαντική ανάπτυξη στα προηγούμενα 15 χρόνια, με τα κελιά καυσίμου να χαρακτηρίζονται εν μέρει από τα μοναδικά χαρακτηριστικά της άμεσης ενεργειακής μετατροπής της χημικής ενέργειας σε ηλεκτρική ενέργεια. Δεδομένου ότι η τεχνολογία κυψελών καυσίμου έχει περάσει μέσω της ανάπτυξης και της προ-εμπορευματοποίησης, υπάρχει αυξανόμενο ενδιαφέρον για τα ζητήματα κατασκευής και εφαρμογής τους.

Από τους έξι διαφορετικούς τύπους κυψελών καυσίμου που κατασκευάζονται εμπορικά, η κυψέλη καυσίμου ανταλλαγής πρωτονίων (PEM) έχει λάβει το μέγιστο ποσό επένδυσης, έρευνας και ανάπτυξης λόγω της καταλληλότητας του σε ποικίλες εφαρμογές. Η κυψέλη καυσίμου μετατρέπει τα καύσιμα όπως το φυσικό αέριο, τη μεθανόλη, τη βενζίνη ή τη βιοαιθανόλη σε καύσιμα πλούσια σε υδρογόνο τα οποία απαιτούνται από την κυψέλη καυσίμου ή την εκάστοτε συστοιχία (stack) για την λειτουργία τους. Τα κελιά καυσίμου ταξινομούνται συνήθως ανάλογα με τον ηλεκτρολύτη τους.

Το πρώτο σημαντικό μέρος της μελέτης της παρούσας μεταπτυχιακής εργασίας είναι η ανάλυση των βασικών αρχών και η ταξινόμηση των κυψελών καυσίμου και ιδιαίτερα της κυψέλης καυσίμου πολυμερικής μεμβράνης (PEM) και των τμημάτων της.

Η πρώτη αναφορά των χρησιμοποιούμενων υλικών των ηλεκτροδίων έγινε επάνω σε μέταλλα λευκόχρυσου και στην χρήση ηλεκτροδίων χαμηλής περιεκτικότητας σε λευκόχρυσο έως και την μη ύπαρξη του στο ηλεκτρόδιο.

Η πειραματική έρευνα έγινε για τους διμεταλλικούς ηλεκτροκαταλύτες Pd_xRh_y και Pd_xPt_y.Τα αποτελέσματα που προκύπτουν από αυτά τα πειράματα παρατίθενται στο κεφάλαιο 4 και στο κεφάλαιο 5.

Επιπλέον, τα πειράματα με την κυψέλη καυσίμου τύπου PEM αναλύονται στο κεφάλαιο 6 της διατριβής και τα αποτελέσματα παρουσιάζουν τη σύνδεση μεταξύ της πυκνότητας ρεύματος και της θερμοκρασίας της κυψέλης καυσίμου καθώς η τελευταία αυξάνεται.

Τα συμπεράσματα και οι προοπτικές για περαιτέρω έρευνα και ανάλυση τόσο πειραματική όσο και θεωρητική παρουσιάζονται στο Κεφάλαιο 7 σαν καταληκτικό κομμάτι της παρούσας διπλωματικής εργασίας.

CHAPTER 1

1. Introduction - Motivation and background

Fuel cells create power by an electrochemical response in which oxygen and a hydrogen-rich fuel are joined to structure water. Not at all like interior combustion engines, the fuel is not combusted, however the vitality is rather being discharged electro-synergistically. This permits fuel cells to be exceedingly vitality productive, particularly if the warmth delivered by the response is likewise outfit for space warming, high temp water or to drive refrigeration cycles[5].A fuel cell is similar to a battery in a manner that creates power from an electrochemical response [6]. Both batteries and fuel cells change over substance potential vitality into electrical vitality furthermore, as a by-result of this procedure, into warmth vitality. Regardless, a battery holds a close store of essentialness inside it and once this is depleted the battery must be discarded, or resuscitated by using an external supply of force to drive the electrochemical reaction in the opposite bearing. A force module, on the other hand, uses an outside supply of compound essentialness and can run always; the length of it is supplied with a wellspring of hydrogen and a wellspring of oxygen (ordinarily air). There are a couple of assorted sorts of vitality segments anyway they are all based around a central design. A vitality segment unit embodies a stack, which is made out of different individual cells. Every cell inside the stack has two anodes, one positive and one negative, called the cathode and the anode. The reactions that make force happen at the terminals [6]. Every power gadget similarly has either a vigorous or a liquid electrolyte, which passes on particles starting with one terminal then onto the next, and an impulse, which enlivens the reactions at the anodes. The electrolyte accept a key part - it must permit simply the fitting particles to pass between the terminals[7]. If free electrons or diverse substances pass through the electrolyte, they disturb the blend reaction and cut down the viability of the cell. Power devices are for the greatest part characterized by

the nature of the electrolyte (with the exception of direct methanol energy units which are named for their capacity to utilize methanol as a fuel), each one sort obliging specific materials and fuel. Each one energy unit sort additionally has its own particular operational attributes, offering focal points to specific applications [7].This makes power modules an exceptionally adaptable innovation. Accordingly, energy units have a more extensive scope of uses than some other presently accessible force source from toys to huge force plants, from vehicles to portable chargers, and from family power to general force [5].

Hydrogen (H_2) is a fuel that can be created from distinctive assets and for residential utilization. Hydrogen is secured up gigantic amounts in water (H2O), hydrocarbons, (for example, methane, CH_4), and other natural materials. One of the difficulties of utilizing hydrogen as a fuel originates from having the capacity to proficiently extricate hydrogen from these mixes[8].

Albeit in its market outset as a fuel, government and industry are working towards clean, efficient, and safe hydrogen generation and dissemination for utilization in transportation and force plants. Hydrogen starts to enter the purchaser advertise in limited locales locally and far and wide [8]gigantic amounts in water (H2O), hydrocarbons, (for example, methane, CH4), and other natural materials. One of the difficulties of utilizing hydrogen as a fuel originates from having the capacity to proficiently extricate hydrogen from these mixes [8].

Fuel cells and especially proton exchange membrane fuel cells use mostly hydrogen as their fuel in order to operate. The basic operation element of this type of fuel cell is platinum and platinum based anodes and cathodes.

Pt reservations and its high price significantly contribute to the total cost of PEMFCs so as not to be as expensive as they are now. Based on this problem, for PEMFCs to become widely known, the challenging issue is to reduce the high cost of the catalyst resulting from the exclusive adoption of Pt or Pt-based catalysts[4]. One of the targets of the scientific community is to reduce the Pt loading or improve the utilization of Pt for optimizing the membrane electrode assemblies (MEAs) structure[7]. Last years, various approaches have been reported in order to lower the cost concerning the

design, fabrication, characterization and testing of novel Pt-free anodes and cathodes for hydrogen PEMFCs applications [4].

Our goal with the current research is to test palladium based anodes and cathodes of a PEMFC in order to test their efficiency and the impact of the absence or the low presence of platinum in the catalysts made [8].

The rest MSc thesis is classified into five more Chapters. More precisely:

In Chapter 2: The aim of Chapter 2 is a quick introduction at the operation basics of fuel cells, a quick view in their historical background and their applications. In sequence a brief historical overview of PEM fuel cells and the state-of-the-art of electrocatalysts that have been studied are also discussed. The role of the catalyst in the proton exchange membrane fuel cell is also studied with the anode and the cathode processes analyzed and with analysis of the role of platinum in the PEM fuel cell.

In Chapter 3: The experimental techniques and their main principles that were used for the physicochemical and electrochemical characterization of the studied electrocatalysts are described.

In Chapter 4: Carbon supported Pd_xRh_x binary electrocatalysts investigated for hydrogen electrooxidation prepared by a modified pulse microwave-assisted polyol method. The physicochemical properties were obtained by X-ray diffraction (XRD) and by transmission electron microscopy (TEM). The electrochemical activity was investigated by the aid of cyclic voltammetry, rotating disk electrode technique and chronoamperometry.

In Chapter 5: Carbon supported Pd_xPt_x binary electrocatalysts investigated for hydrogen electrooxidation prepared by a modified pulse microwave-assisted polyol method. The physicochemical properties were obtained by X-ray diffraction (XRD) and by transmission electron microscopy (TEM). The electrochemical activity was investigated by the aid of cyclic voltammetry, rotating disk electrode technique and chronoamperometry.

In Chapter 6: In Chapter 6, an electrochemical characterization of the homemade fuel cell MEA is made. The used membrane is $Pd_{97}Pt_3/C$. The measurements before the catalytic activation of the MEA are presented and the chapter concludes with the

presentation of the distinctive polarization curves of the fuel cell regarding measurements in different temperatures.

In Chapter 7: The conclusions and future perspectives are summarized in Chapter 6. For hydrogen electrooxidation Pt is a very suitable catalyst due to its high efficiency and its poor selectivity of different substances presented in physiological solutions. Preparation method is a very important parameter for catalysts' preparation as it affects their properties (lattice parameter, diameter of nanoparticles, catalysts dispersion on the support). A modified microwave assisted polyol method was chosen because of the following remarkable advantages: i) rapid volumetric heating, ii) higher reaction rate and selectivity, iii) shorter reaction time and iv) higher yield of the product compared to the convention heating methods. Moreover, replacing one part of Pt with Pd and developing Pd-based electrocatalysts with different preparation methods reduces at a great percentage the fuel cell's cost. Thus, catalysts preparation methods should be further optimized.

CHAPTER 2

2. THEORETICAL BACKROUND

The aim of Chapter 2 is to provide a quick introduction to the technology of fuel cells, and a quick view to their background and their applications. Then a thorough discussion is done about the electrolytes and the existing types of fuel cells. Among fuels, hydrogen, methanol and ethanol, that can be used in alkaline and proton exchange membrane fuel cells hydrogen is considered to be a fuel with perspectives for the development of fuel cells. Furthermore, electrodes and their properties are reported in terms of the used catalysts. The anode and cathode electrocatalysts for hydrogen fuel cells are analytically reported. Furthermore, in this chapter an introduction is made about the use of platinum and the amount of it as electrocatalysts in a PEMFC. PEMFCs currently use Pt as the catalyst both at the cathode and the anode, for reasons which will be described in the chapter below. Recent analyses indicate that Pt would be around 17% of the total cost of an 80 kW PEMFC system using 2012 technology at mass production scale[4]. Naturally there is interest in developing substitute catalysts based on cheaper metals, although any other catalyst developed would need to exceed Pt in terms of performance against total system cost.

This chapter focuses on the fundamentals that are required for an idealized PEM fuel cell electrode material and evaluates the performance of pure Pt anodes and cathodes compared to the low platinum electrocatalysts and the platinum free electrocatalysts that can be used in a PEM fuel cell.

2.1 Operation basics – Definitions – History of fuel cells

The primary fuel cell was fabricated and showed in 1839 by Sir William Robert Grove, FRS (Fellow of the Royal Society), expanding upon the work of the German scientist Christian Schonbein. Grove tried his hypothesis by encasing two platinum strips in divided fixed containers, by which the one contained hydrogen and the other contained oxygen individually shaped by preparatory electrolysis of the electrolyte[9]. When these containers were immersed in diluted sulfuric acid, a current began to flow between the two electrodes and water was formed in the gas bottles. The invention, which later became known as a fuel cell, did not produce enough electricity to be useful[10]. Three years later, Grove showed that he was already well aware of the fact that the three phase contact is essential: “As the action could only be supposed to take place with ordinary platinum foil, at the line or water-mark where the liquid, gas or platinum met” [11]. He extended this contact by coating the electrodes with “spongy platinum”. Shortly after, Grove reported on a hydrogen-chlorine fuel cell and he found that “other volatile bodies such as camphor, essential oils, ether and alcohol associated with oxygen gave a continuous current. It can be said that the very first fuel cell invented by Grove foreshadowed the phosphoric acid fuel cell (PAFC) of more recent date. Unfortunately for the early introduction of fuel cells, the development of the dynamo technology in 1866 by Werner Von Siemens overshadowed the discovery of this promising energy converter [6].

William White Jaques was the first analyst who utilized phosphoric corrosive acid as a part of the electrolyte shower and he instituted the expression "fuel cell"[12].

An important step forward in the development of the H_2-O_2 fuel cell became with Mond and Lager [13, 14]. They found, as Grove had observed, that the efficiency of the platinum black coating of the electrodes was soon lost if it became wet. Thus, they constructed a fuel cell with a diaphragm from plaster of Paris, earthenware, asbestos or pasteboard, impregnated with dilute sulfuric acid. The electrodes of thin perforated platinum foil, coated with platinum black, were placed onto the dry backside[9]. The efficiency was calculated to be 50% of the heat of combustion. Also, stacks of cells in parallel were constructed.

Francis Thomas Bacon at first explored different avenues regarding Grove's utilization of enacted platinum bandage with a sulfuric corrosive electrolyte, yet immediately proceeded onward, to utilize actuated nickel terminals with a watery potassium hydroxide electrolyte[15]. At that point he built up a twofold cell, with one unit for creating the hydrogen and oxygen gases and the other for the power module. That could be turned around so it went about as both an electrolyser and a power device. Issues were experienced because of the high working temperatures and weights and the destructive way of the chemicals.

After that, Bacon's group utilized permeable nickel sheet to create anodes with substantial pores on the gas side and better ones on the electrolyte side, which made a significantly more steady interface than had existed already. The team overcame problems of corrosion of the oxygen electrode by soaking the new nickel electrodes in lithium hydroxide solution followed by drying and heating[16]. In 1959, with backing from Marshall of Cambridge Ltd a welding machine bolster by a 5 kW forty-cell battery, with a working effectiveness of 60%, was shown openly.

Pratt and Whitney thusly authorized the outline to power the Apollo space vehicle, an enhanced variant of which supplies power for the Space Shuttle [17]. With the space missions the fuel cell found its first real application. At around the same time, Harry KarlIhrig fitted a modified 15 kW Bacon cell to an Allis-Chalmers agricultural tractor. It was fed by propane, an available fuel that is rich in hydrogen and as it burns it produces oxygen, blue flame and is poor in carbon dioxide. Allis-Chalmers, in partnership with the US Air Force, developed a number of fuel cell powered vehicles including a forklift truck, a golf cart and a submersible vessel[18].

Fuel cells are inherently modular and therefore lend themselves to a wide range of applications. They can be categorized into three broad areas: portable power generation, stationary power generation, and power for transportation.

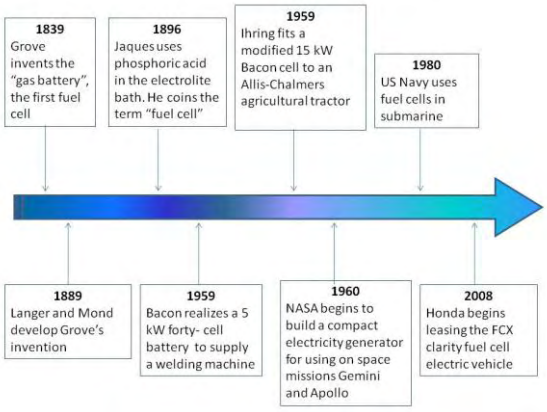

Figure 2.1. History and development of fuel cells[17, 19].

Stationary power plants

Stationary fuel cells are units which provide electricity (and sometimes heat) but are not designed to be moved. These include combined heat and power (CHP), uninterruptible power systems (UPS) and primary power units. CHP units are sized between 0.5 kW and 10 kW, use either PEM or SOFC technology and take advantage of the fact that fuel cells generate heat alongside with electricity [2, 20]. UPS systems provide a guaranteed supply of power in the event of grid interruption; this market can be divided into five sub-sectors:

- logged off short run-time frameworks for telecom base stations;
- logged off augmented run-time frameworks for basic correspondence base stations, for example, Terrestrial Trunked Radio (Tetra) systems;
- disconnected from the net developed run-time rack mountable frameworks for server farms;
- on-line rack mountable frameworks for server farms;
- Disconnected from the net frameworks for private utilization.

In Japan more than 2000 homes are utilizing power devices as another ecological force producing innovation[2].

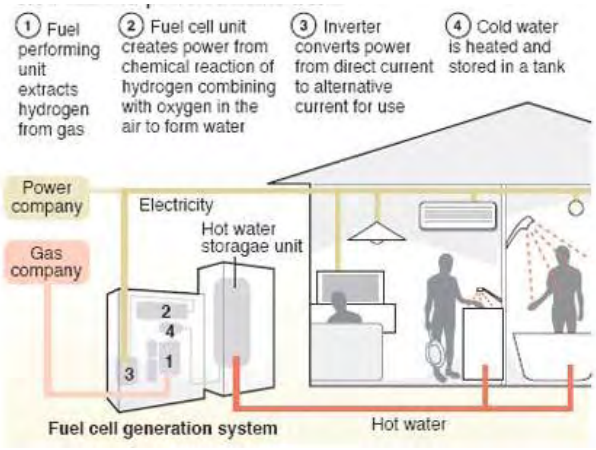

Figure 2.2. Fuel cell powered home works[21].

Portable power plants

Portable fuel cells are built into, or charge up, products that are designed to be moved. These include military applications (portable soldier power, skid mounted fuel cell generators etc.), Auxiliary Power Units (APU) (e.g. for leisure and trucking industries), portable products (torches, vine trimmers etc.), small personal electronics (mp3 players, cameras etc.), large personal electronics (laptops, printers, radios etc.), education kits and toys [2]. To power this range of products, portable fuel cells are being developed in a wide range of sizes ranging from less than 5 W up to 500 kW. The main drivers for fuel cells in portable applications are:

- off grid operation;
- longer run-times compared with batteries;
- rapid recharging;
- significant weight reduction potential convenience (for soldier-borne military power);
- reliability and lower operating costs[2].

Transportation

Fuel cells can provide propulsive power to a vehicle, directly or indirectly.

These include the following technology:

- forklift trucks and other handling vehicles such as airport baggage trucks etc;
- Two/ three-wheeler vehicles such as scooters;

- light duty vehicles (LDVs), such as cars and vans;
- buses and trucks;
- trains and trams;
- smaller boats and ferries;
- light aircraft;
- unmanned aerial vehicles (UAVs) and unmanned undersea vehicles (UUVs), for example, for reconnaissance[2].

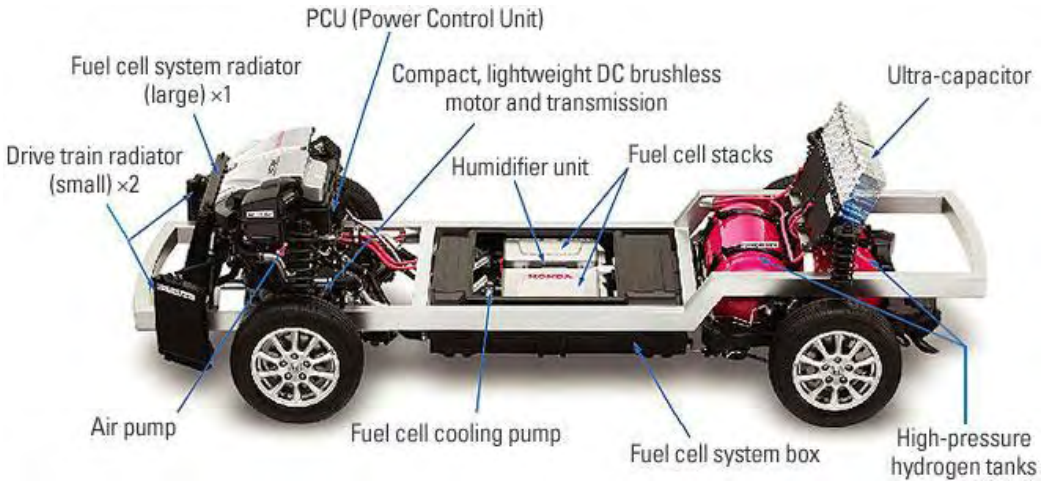

Figure 2.3. Components in a fuel cell car[12].

Fuel and infrastructure

Base identifies with the supplies and frameworks expected to deliver, appropriate, store, screen and administer the fuels, particularly hydrogen, for fuel cells. Most types of fuel cells oblige hydrogen as a fuel source. The long haul objective of energy unit examination is to deliver a completely non-dirtying force source. Keeping in mind the end goal to accomplish this, the fuel cell must run on hydrogen created by renewable means.

The innovation to do this does exist, however the framework to attain to this proficiently and inexpensively is still being worked on. Besides, fuel cells can be controlled by hydrogen extricated from fossil powers (oil and natural gas) by reorganization. Transforming can either occur on a vast scale at source, or generally by utilizing little reformers incorporated with the fuel cell [22].

Structure of fuel cells

Regardless of the mixed bag of fuel cell devices, they all work in the same general way. They are comprised of three nearby portions: the anode, the electrolyte and the cathode. Two compound responses happen at the interfaces of the three separate portions. The net consequence of the two responses is that fuel is expended, water or carbon dioxide is made, and an electric ebb and flow is made, which can be utilized to power electrical gadgets, typically alluded to as the load. At the anode, an impetus oxidizes the fuel, normally hydrogen, transforming the fuel into an absolutely charged particle and a contrarily charged electron [23]. The electrolyte is a substance that is particularly planned so particles can go through it and electrons will be blocked. The liberated electrons go through a wire, making the electric current. The particles make a trip through the electrolyte to the cathode. There, the particles are brought together with the electrons, and these two respond to make water or carbon dioxide. Energy components have been utilized for more than 150 years, in spite of the fact that for a few decades they have been slipped out of spotlight.

There are various sorts of power gadgets, yet they all involve two metallic (e.g. platinum) terminals dove into an electrolyte game plan. In a working power gadget, the negative terminal, the anode, produces electrons by "seething" a fuel. The positive terminal, the cathode, ingests electrons in diminishing an oxidizing expert. The fuel and the oxidizing expert are each one supplied to its terminal [24]. It is basic starting at this time to make conditions that they not one or the other mixing no particularly the reactants or supply the "wrong" terminal with the "wrong" fuel. To reject unintentional contact between the anode and the cathode (which would make an internal short at the cell), an electronically ensuring porous separator (holding an electrolyte plan that sponsorships current transport by particles) is oftentimes situated into the gap between these terminals. In any case, the cell circuit continues being closed [25].

Receiving the exceptionally fundamental grouping of directing materials presented by Faraday in 1834, the electrodes are conductors of the first kind (electron conductors) and the electrolyte is a conductor of the second kind (particle conductor)[24]. The main of the two electrodes is assigned as "anode" and the alternate as "cathode". The

cathodes are connected on the two free surfaces of the electrolyte with the goal that the phone can be typically composed as:

‘’Anode’’ / “Electrolyte” / ‘’Cathode’’,

Where "/" speaks to a cathode/electrolyte interface. One of the terminals is persistently nourished by the fuel and the other is presented to an oxidative medium (most generally to climatic air) and they are both joined with one another through an outer electrical circuit [24].

By alluding to the meaning of electrical current as "arranged movement of electrons", and also that the electrolyte is a transmitter of the second kind, one can without much of a stretch watch that the electrical circuit can't work without the presence of a fitting component of charge (electrons) exchange through the electrolyte. For all intents and purposes, this system relates to the relocation of particles (charge bearers) from one terminal to other - because of a fixation angle - which is proportionate to the electrical current.

The designation of an electrode as “anode” or “cathode” relies on the direction of the electrical current traversing through the electrode/electrolyte interface. Taking into account that the direction of electricity is, by convention, opposite to the direction of the electronic motion, the current is positive ($I > 0$) and is called “anodic” when it traverses from the electrode to the electrolyte. Therefore, the electrode is designated as “anode” by a positive sign (+) when is traversed from “anodic” current and the other electrode is “cathode” represented with a negative sign (-). This conventional designation is absolutely arbitrary but convenient [26].

Fuel cells are a group of advancements that produce power through electrochemical procedures, instead of ignition. There are numerous energy component sorts, however the key ones incorporate the basic alkaline fuel cell (AFC), proton exchange membrane (PEM) fuel cell, direct methanol fuel cell (DMFC), molten carbonate fuel cell (MCFC), phosphoric acid fuel cell (PAFC) and solid oxide fuel cell (SOFC). Many of these fuel cell types are financially accessible today.

Every fuel cell device has its own particular novel science, for example, distinctive working temperatures, impetuses, and electrolytes. An energy unit and its working

qualities help characterize the application. The most widely recognized kind of energy component is the proton exchange membrane fuel cell with incredible research been carried out in the previous years.

Environmental impact

Fuel cells have very low environmental impact, particularly when compared to other devices of power conversion. The only product of the electrochemical reactions is water or CO_2(with organic fuel) at very low concentrations. Moreover, the use of low temperatures avoids other side reactions involving pollution by products (nitrogen and sulphuric oxides, etc). Another important advantage is the use of bio-alcohols. Methanol and ethanol can be used in the so-called Direct Methanol Fuel Cells or Direct Ethanol Fuel Cells (DMFCs, or DEFCs, respectively). Since alcohols can be obtained from renewable sources, this process of energy conversion is sustainable [27].

Even though hydrogen is one of the most abundant elements found on Earth, hydrogen gas (H_2) is very limited in the atmosphere. The methods and sources employed for the production of H_2 usually involves the use of fossil resources (natural gas) and other non-sustainable processes. Such methods demand high economic and technological efforts. Alternative methods to produce or store hydrogen are still under research. Interest has focused on the development of devices to produce hydrogen from renewable sources, using hydrogen as an energy vector [27].

In the following sub-section the proton exchange membrane fuel cells are described more detailed.

2.1. Proton exchange membrane fuel cells (PEMFCs)

The proton electrolyte fuel cells consist of an anode, on which the oxidation of hydrogen occurs, a cathode, where oxygen reduction occurs and a polymeric electrolyte, assembled to constitute the so-called MEA (Membrane Electrode Assembly) [28].

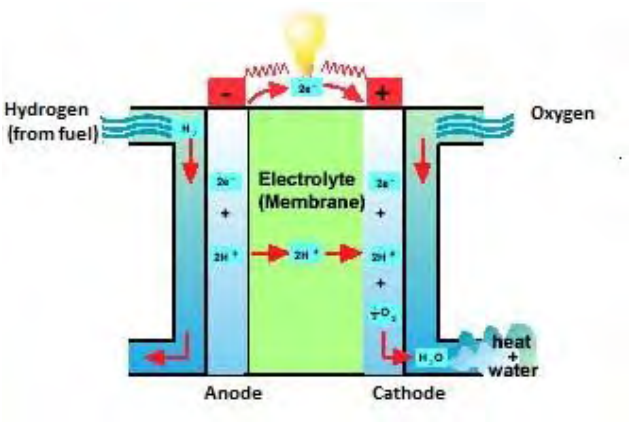

Figure 2.4. Scheme of a proton exchange membrane fuel cell[26].

The MEA consists of a proton exchange membrane, catalyst layers (CL), and gas diffusion layers (GDL). In PEMFCs, as in many other types of fuel cells, gas-diffusion electrodes are used. Gas Diffusion Layer (GDL) is a very important supporting material in a MEA, the heart of a fuel cell.

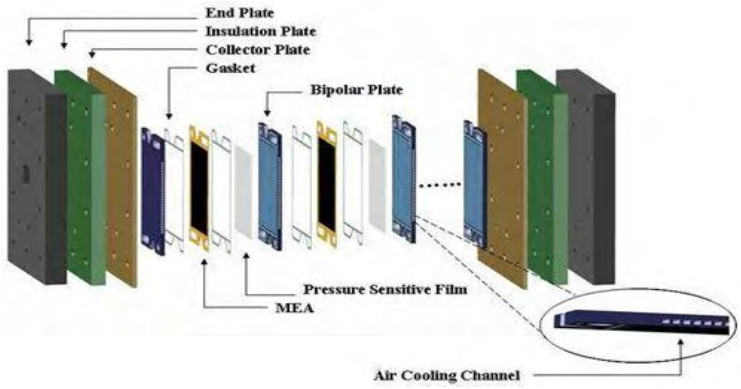

Figure 2.5. Components of a fuel cell[19].

GDL serves as a ''bridge'' between the MEA and the graphitized plates. The main functions of GDL are:

1. A gas diffused pathway from the flow channels to the catalyst layer.
2. Remove the produced water outside of the catalytic layer and prevent flooding.
3. Keep water on the surface for conductivity through the membrane.
4. Helps the heat transfer while the cell operates.
5. Provide enough mechanical strength to hold MEA from extension caused by water absorbance.

The catalytic layer (CL) is located between the PEM and the gas diffusion layer (GDL). Protons are transferred between the CL and the PEM, and electrons are transferred between the catalytic layer and the GDL[29].Both require good interfacial contact. In a PEM fuel cell, the CLs' are located where the electrochemical reactions occur for power generation[28].

The basic requirements for a catalytic layer include[30]:

- A substantial number of three-stage limit locales;
- Efficient transportation of protons from the anode reactant layer to the cathode synergist layer;
- Easy transportation of reactant gasses to the synergist surface;
- Efficient water administration in the CLs';
- Good electronic current entry between the response locales and the current collector.

Every cell is differentiated from its associated cell by an electronically directing bipolar plate. This plate is in contact on the one side with the positive terminal of a given cell and on the other side with the negative cathode of the neighboring cell. Such plates in this way, work as interconnections for cells joined in arrangement, much the same as in a battery. The bipolar plate has channels that are removed on both sides, which by means of manifolds are supplied with the reactant gasses (hydrogen and oxygen)[5]. The gases are carried to the electrodes by these channels. Such channels serve to eliminate water vapor as a reaction product from the oxygen side. Between any two bipolar plates providing access to the reactant gases, a MEA is set up that consists of a positive electrode and a negative electrode pressed into the two sides of a proton-conducting membrane.

The membranes play a crucial role in the operation of the PEM fuel cells. They are responsible for:

i. separate fuel from the oxidant,
ii. exhibit a high proton conductivity (allow the transportation of protons with as meager resistance as could be expected under the circumstances),
iii. poorly leading the electrons,
iv. have low gas penetrability.

2.2. Electrodes: types and properties

Electrodes act as catalytic sites for reactions that consume fuels and oxidizers, with production of water and flow of current in the external circuit[21].

Anode and cathode electrodes are two important constructive elements of fuel cells, serving to the accomplishment of highly selective processes during their operation. Electrodes must be materials of high electronic conductivity (conductors of the first kind) in order to collect and transfer electrons with minimum ohmic losses and minimum impact to the efficiency of the cell [21].

The most crucial requirements for the design of electrodes can be summarized as follows:

- they must have high electronic conductivity;
- high synergist action;
- the capacity for particles to simple relocate in their interfaces with electrolyte (low charge exchange coefficients);
- thermal and mechanical steadiness amid operation;
- they ought to have minimal cost;
- adequate porosity;
- existence of fitting methods for their application on the electrolyte [31].

Practically speaking, the synchronous satisfaction of all above necessities by one anode material is a case unimaginable or uncommon. A trade off is normally received in the middle of lavish and very compelling materials, for example, noble metals and modest however less dynamic anodes made of regular metals, for example, perovskites or different materials. Some vital parameters, then again, are normally the operation temperature of the cell and the resistance to ruinous impacts like harming. In low temperature power modules, (for example, PEMFCs, AFCs and PAFCs), response energy requires very successful cathodes, for example, Pt. Then again, high temperature applications (i.e. in SOFCs) force loose necessities for movement since response energy is decidedly impacted [21].

2.3. Role of catalyst in PEM fuel cell

Pt is used as a catalyst for both hydrogen oxidation reaction (HOR) occurring at the anode and oxygen reduction reaction (ORR) at the cathode.

2.3.1. Anode processes

Hydrogen flows into the fuel cell and reaches the Pt anode where the HOR (hydrogen oxidation reaction) takes place. Here the hydrogen adsorbs onto the surface of the Pt electrode, breaking the hydrogen-hydrogen bond to give adsorbed atomic hydrogen (H*):

$$½\ H_2 + * \rightarrow H^* \quad (1)$$

Where * denotes the surface site.

Subsequent loss of an electron from each adsorbed hydrogen leads to hydrogen leaving the surface as protons (H^+):

$$H^* \rightarrow H^+ + * + e^- \quad (2)$$

In a PEMFC, the kinetics of the HOR on a Pt electrode is very fast. Voltage losses are extremely small even for very low Pt loadings. As the HOR is fast, the main focus of catalyst improvement has always been on the cathode process.

Platinum Supply & Demand (2011-2013, '000 oz)			
Supply	**2011**	**2012**	**2013**
South Africa	4,860	4,090	4,120
Russia	835	800	780
North America	350	310	315
Zimbabwe	340	340	400
Others	100	110	125
Total Supply	**6,485**	**5,650**	**5,740**
Demand			
Autocatalysts	3,185	3,190	3,125
Jewelry	2,475	2,780	2,740
Industrial	1,975	1,605	1,790
Investment	460	455	765
Recycling	-2,060	-2,040	-2,075
Total Demand	**6,035**	**5,990**	**6,345**
Stocks	**450**	**-340**	**-605**
Source: Johnson Matthey's Platinum 2013 Interim Review			

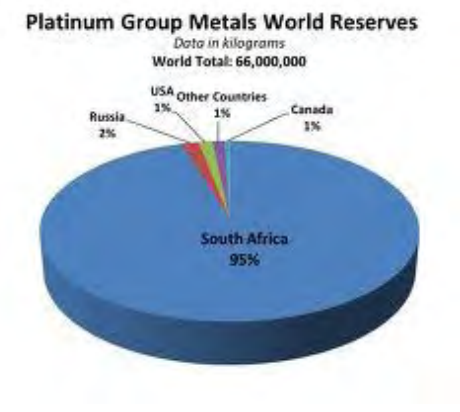

Figure 2.6. Platinum supply and demand (2011-2013) and graph related to the platinum group metal world reserves[2].

Cost targets for PEM penetration into the automotive area are constrained by the price and supply of platinum. Over 50% of the cost of a fuel cell is dominated by the cost of the electrodes. Today, in order to reduce the cost of H2-PEMFCs, great effort has been devoted by a number of research groups world-wide in order to decrease the Pt loading

at a level of 200 mgPt_{tot} kW^{-1} or <5 mW$\mu g^{-1}Pt_{tot}$ as it has been expressed by the DOE of the USA (until 2015).

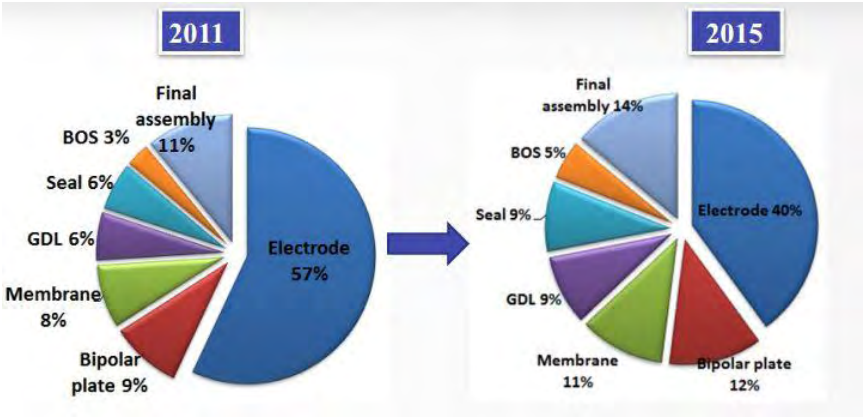

Figure 2.7. Cost of a fuel cell 80 kW[4].

2.3.2. Cathode processes

The ORR is well recognized as sluggish. The slow kinetics constitutes one of the major voltage losses due to the high reduction overpotential in the performance of a PEMFC. The ORR is the major challenge for PEMFCs because the catalyst material must be stable under the extremely corrosive conditions at a fuel cell cathode yet chemically active enough to be able to activate O_2. In addition it must be noble enough for facile release of product water from the catalyst surface in order to free up catalytic sites once the reaction is complete. Due to the difficulties of the ORR, the cathode requires a higher Pt loading, typically more than several times that of the anode[32]. There are two pathways by which ORR can occur in acidic media. The first mechanism is the preferred dissociative pathway and follows a concerted 'four electron' transfer process leading to direct formation of water. First O_2 adsorbs to the metal surface and the oxygen–oxygen bond breaks to give adsorbed oxygen atoms (O*):

$$½\ O2+* \rightarrow O* \qquad (3)$$

These single oxygen atoms are then protonated by the incoming flow of H+ across the PEM and reduced by incoming flow of electrons to give surface bound hydroxyl (OH*) groups:

$$O*+H^{+}+e^{-} \rightarrow OH* \qquad (4)$$

The surface bound OH* is then further reduced and protonated to give water which then leaves the metal surface:

$$OH^*+H^++e^-\rightarrow H2O+^* \quad (5)$$

The alternative pathway is an associative mechanism where the O=O bond does not break upon O_2 adsorption onto the metal surface:

$$O_2+^*\rightarrow O_2^* \quad (6)$$

$$O_2^*+H^++e^-\rightarrow HO_2^* \quad (7)$$

This option 'two electron' course is seen to deliver H_2O_2. The subtle elements of the component are misty, yet the response may move ahead as takes after:

$$HO_2^*+H^++e-\rightarrow H_2O_2^* \quad (8)$$

The H_2O_2 respond further or desorb

$$H_2O_2^*\rightarrow H_2O_2+^* \quad (9)$$

Generation of H_2O_2 in a PEMFC is exceedingly undesirable as it diffuses into the PEM and results in radical oxidative corruption of the layer [32].

Required characteristics of the catalyst for PEMFC:

There are four main characteristics that are essential for an effective PEMFC catalyst:

- Activity: to be able to adsorb the reactant strongly enough to facilitate a reaction but not so strongly that the catalyst becomes blocked by the reactant or products (*Sabatier principle*).
- Selectivity: to make the desired product and minimize the production of undesirable intermediates and side products.
- Stability: to withstand the operating environment in a fuel cell, including strong oxidants, reactive radicals and acidic environment at high and rapidly fluctuating temperatures, all whilst under an applied voltage.
- Poisoning resistance: to be resistant to poisoning by impurities likely to be found in the fuel cell itself and in the feed gases.

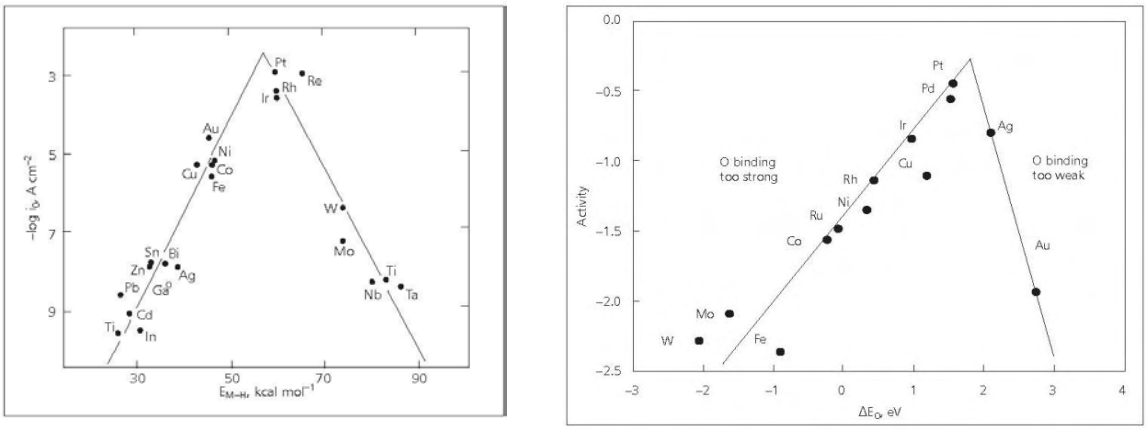

Figure 2.8. Schematic representation of Sabatier principle [1].

2.4. Low platinum and platinum free electrocatalysts for PEMFCs'

Platinum is the basic catalyst for electrochemical reactions at hydrogen and oxygen electrodes in three of six main fuel cells types (PEMFC, DMFC and PAFC). Platinum is rare and is mined in a limited number of countries worldwide, with >75% mined in South Africa, for this reason its price is very high and its cost limits fuel cells' commercialization. In the first models of membrane fuel cells, the dispersed platinum catalyst was in a pure form, so that large amounts of platinum were used [33].

Significant research has been focused on reducing and removing platinum from these systems. In a wide variety of catalytic uses, platinum offers benefits in terms of activity and selectivity which cannot be achieved using alternating materials. This is the case in fuel cells, where for both the oxygen reduction reaction (ORR) and the hydrogen oxidation reaction (HOR), the activity and selectivity of platinum exceeds that of all other materials [34].

Most H_2-PEMFCs have adopted Pt as HOR and ORR material, but as it is aforementioned Pt reserves are not enough and its price is very high. In this section, it is reported and discussed the research and development of the last decade devoted to low-platinum PEMFCs' anode and cathode electrocatalysts for Hydrogen Electro-oxidation Reaction (HOR) and Oxygen-reduction reaction (ORR).

Many different techniques have been adopted in order to reduce Pt loading in PEMFCs, such as: sputter deposition [35], hydrothermal method[36], electrospinning and chemical dealloying techniques [37], thin film method[7], etc. In this sense, platinum alloys are considered as a plausible solution. The combination of Pt with another metal can improve the electrocatalytic activity. Another effective way to

decrease Pt loading is the adoption of high specific surface area supports to enhance both Pt dispersion and utilization coefficient [38].

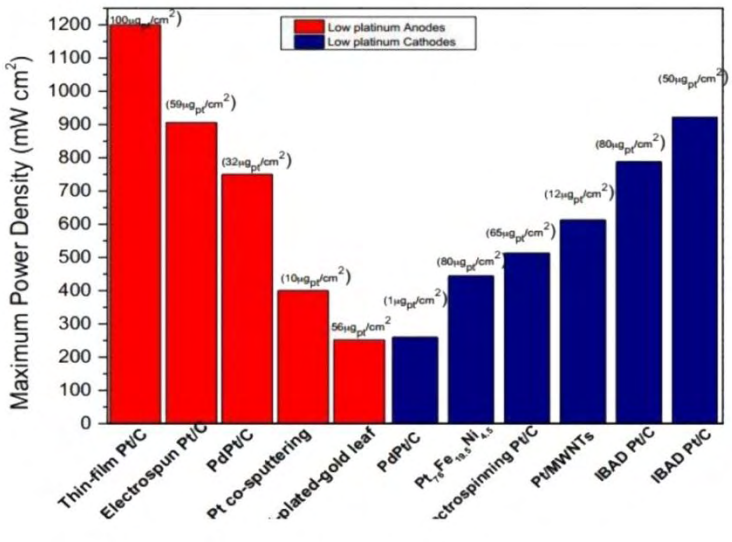

Figure 2.9. Results of the recently appeared investigations concerning different techniques that are used for the preparation of low platinum anodes and low platinum cathodes for H_2-PEMFC [4].

A three step electrodeposition process was adopted by the researchers for the preparation of a PtFeNi catalyst with an ultra-low Pt loading of 50 μgPtcm^{-2} which exhibited good performance and stability. Mougenot et al. [39] prepared a MEA with an ultra-low Pt loading made by pure Pd anode and PdPt cathode deposited on commercial carbon woven web and carbon paper GDLs by plasma sputtering, that under fuel cell operation performed 250 mWcm^{-2}.

The following figure summarizes all the results reported in the international literature the last decade, concerning both low Pt anodes and low Pt cathodes with total Pt loading with less than 5 mWμg^{-1} as it has been expressed by the DOE of the USA (until 2015).

2.4.1. Anodes and cathodes

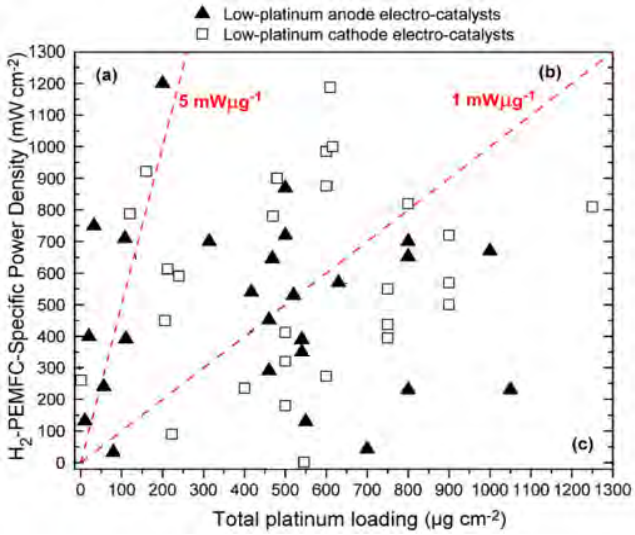

Figure 2.10.H_2-PEMFC operation results: maximum power density (mW cm^{-2}) dependency on total (anode & cathode) Pt loading (μg cm^{-2}) [4].

As it can be seen from the diagram above, the results can be classified in three regions of maximum mass specific power densities values: a) higher than 5 mW μg^{-1}_{Pttot}, b) between 1 and 5 mW μg^{-1}_{Pttot} and c) lower than 1 mW μg^{-1}_{Pttot}. The reported maximum power density close to 906 mWcm^{-2}, has been recorded by Pintauro et al. [40] over nanostructured fuel cell electrodes. More precisely they fabricated a MEA with both anode and cathode Pt loading of 114 μg cm^{-2}, by using electrospinning technique with a superior catalyst utilization and long-term durability. Sung et al. [41] achieved a MSPD of 750 mW cm^{-2}; 32 μg_{Pt} cm^{-2} with 23.5 mWμg^{-1} by containing PdPt/C anode electrocatalyst and Pt/C cathode. A carbon supported PdPt catalyst with Pd:Pt atomic ratio of 19:1 was synthesized as anode by the sodium borohydride reduction method combined with freeze-drying. The Pt loading was only 5% Pt indicating that Pd can successfully enhance the cell performance. Mukerjee et al.[42] also reported interesting H_2-PEMFC's performance values that exceeded the DOE's 2015 target (6.56 mW $\mu g^{-1}_{Pttotal}$ or 788 mW cm^{-2}) using a MEA with 120 μgPt cm^{-2} of total platinum loading. Their MEA consisted of Pt alone and the electrodes were obtained by direct metallization of non-catalyzed gas diffusion layers via dual ion beam assisted deposition (IBAD) method. Due to this significant improvement, Mukerjee et al. [42]also adopted the same method for the preparation of MEA with Pt alone, as the electrocatalyst, with a total loading of 160 μgPt cm^{-2} and mass

specific power density ca. 5.8 mW $\mu g^{-1}_{Pttotal}$ (or 922 mW cm^{-2}). Summarizing, a great deal of attention has been given not only to Pt alloys but also to the electrocatalyst preparation methods and support identification. Thus, so far, there is an improvement in H_2-PEMFCs electrocatalysts, with some of them to present maximum mass specific power density values higher than 5 mW $\mu g^{-1}_{Pttotal}$.

Antolini et al. [43] also examined Pd-based catalysts. According to their results the MPSD was 6,57 mW$\mu g^{-1}_{Pttotal}$ (710 mW cm^{-2}). The electrocatalysts were prepared by the reduction of metal precursors with formic acid, managing a total platinum loading of 108 μg_{Pt} cm^{-2} (96:4 atomic ratio of Pd:Pt) using a modified thin-film method. Manthiram et al. [44] fabricated a high performance MEA (1200 mW cm^{-2}, 200 μgPt cm^{-2}). The anode and the cathode catalysts were Pt supported on carbon black with a loading of 100μg cm^{-2} for each electrode. Cavarroc et al. [45] manufactured ultra-low Pt content MEA (10 μg cm^{-2} for the anode and 10 μg cm^{-2} for the cathode) by magnetron co-sputtering of carbon and Pt on a commercial E-Tek uncatalyzed gas diffusion layer, which gave a power density of 400 mW cm^{-2} or 20 mW $\mu g^{-1}_{Pttotal}$.

Additionally, Gruber et al. [46]also sputter-deposited Pt thin film layers onto different porous electrodes, as the platinum thin film layer presents the advantage to be active in the immediate neighborhood of the electrode with the proton-conducting membrane. The total Pt loading was only 10 μg cm^{-2} and the maximum mass specific power density almost reached 13.2 mW$\mu g^{-1}_{Pttotal}$ (132 mW cm^{-2}). To reduce Pt loading, except for the trend to alloy the Pt or to modify its support, a proper MEAs fabrication method could also be a promising way. Erlebacher et al. [47] succeeded to control very low values of Pt loading (56 μg cm^{-2} of total platinum loading) by adopting a stamping technique and then to fabricate Pt-plated nanoporous gold leaf, which is a carbon-free electrocatalyst. Despite of the very low Pt amount, they obtained 4.28 mW $\mu g^{-1}_{Pttotal}$ (240 mW cm^{-2}). An optimized electrode structure has been obtained by Mougenot et al. [10]with a Pt loading of 1 $\mu g_{Pttotal}$ cm^{-2}. A H_2-PEMFC, with a cathode of PdPt and an anode made by pure Pd, both deposited on different backing layers by the plasma sputtering technique, exhibited a performance of 260 mW $\mu g^{-1}_{Pttotal}$, which is the highest MSPD reported in the literature.

This result indicates the importance of not only the alloying effect but also the MEAs' fabrication method it is deduced that in the last years one of the common approaches to succeed the Pt loading target was to adopt also novel supports, except carbon black. Among the most examined supports, are the multi-walled carbon nanotubes (MWCNTs) and single-walled carbon nanotubes (SWCNTs), which possess desirable properties as the Pt supports, such as high electrical and thermal conductivity, inertness, etc.

2.5. Platinum free electrocatalysts for H_2 – PEMFC

2.5.1. Anodes

In the recent years, considerable progress has been achieved in developing non-platinum electrodes; however there are only few reports on H_2-PEMFC with Pt-free anode catalysts. Even in these cases the cathode was loaded with Pt. A successful anode catalyst should combine high HOR activity with good long-term stability, a major challenge in the strongly acidic environment of the PEMFC anode. The last decade's efforts for the replacement of the expensive and scarce Pt by non-Pt electrocatalysts in PEMFC anodes is depicted in fig. as one can distinguish in fig4.6, the highest performance of Pt-free anode was achieved by Janxin Ma et al. [48] who prepared highly dispersed non-platinum catalyst based on Ir and Ir-V nanoclusters for PEMFC anode via ethylene glycol method, which at 0,512 V exhibited about 563 $mWcm^{-2}$. This material is expecting to be very promising candidate as platinum alternative anode catalyst. Hyuk Chang et al. [8] over a Pd_3Au/WC catalyst achieved a performance of 238 $mWcm^{-2}$, which was the second best value after the iridium vanadium alloy. Lee et al. [49] prepared and investigated Pd-Ni alloy supported on tungsten carbide; the strong interaction between PdNi alloys and WC caused a performance of 230 mW cm^{-2}. The Pt loading of the cathode electrocatalyst was 300 μg cm^{-2}. Concerning the PdNi/WC electrocatalyst it is worthy to be noticed that there was no obvious performance degradation after 100 h of continuous operation, indicating a long-term stability.

A very common approach to develop non-noble electrocatalysts is to adopt carbides and nitrides. Especially, molybdenum and tungsten carbides and nitrides – cheaper substitutes of Pt-based catalysts – are the most common non-Pt electrocatalysts. The

capability of using transition metal carbides and nitrides for HOR has been investigated since the end of sixties by Bohm and Pohl. It has been shown that tungsten carbide/carbon catalyst can be used in fuel cells operated with hydrogen or CO-rich hydrogen fuel. In order to overcome the Pt loading problem, Kaninski et al. [50] investigated Co (Co/Carbon paper), which costs much less than Pt.Though, the performance of Co towards HOR – not as good as that of Pt – it is higher than that of some other electrocatalysts. Usually, non-precious metal alloys are not preferable from the research community, because the requirement of good resistance to CO is difficult to be achieved. Zhang et al. [51] examined transition metal sulphides (RuS_2/C) for HOR under fuel cell operation and they measured the third better maximum power density value as shown in Fig. 4.6 The cathode's Pt loading was also relatively low (340 μgPt cm^{-2}) and the fuel cell performance reached 100 mW cm^{-2}.

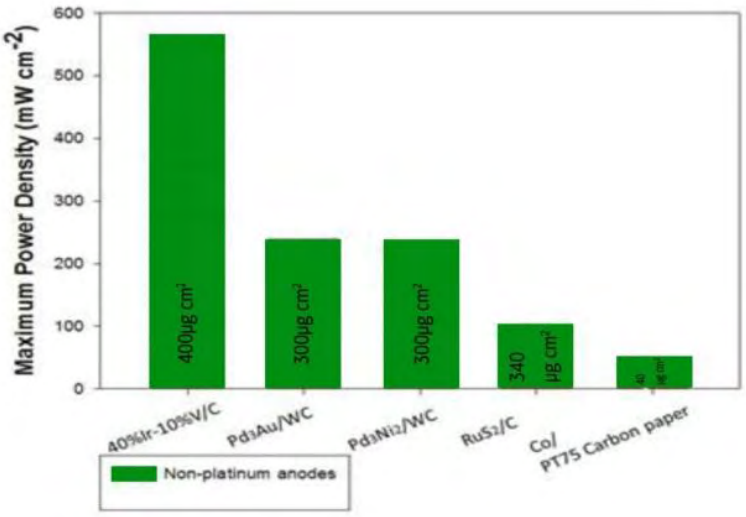

Figure 2.11.H_2-Fuel cell operation over non-platinum anodes: maximum power density (mW cm^{-2}) over different Pt-free anodes. In the brackets is reported the total platinum amount (μg cm^{-2}) contained in the cathode[4].

2.5.2. Cathodes

The last decade, a large number of investigations have also appeared regarding the replacement in fuel cells' cathodes, aimed at the enhancement of the activity towards ORR, which is much slower than HOR. The highest performance reported in the literature for non-platinum cathode in H_2-PEMFC, is 529 mW cm^{-2} achieved by N. Popov et al. [52] over Co-Fe-N chelate complex on the support, followed by chemical

leaching. The maximum power density of 517 mW cm^{-2} obtained by 40% Ir-10% V/C as the cathode catalyst and 400 μg cm^{-2} Pt anode loading [41].

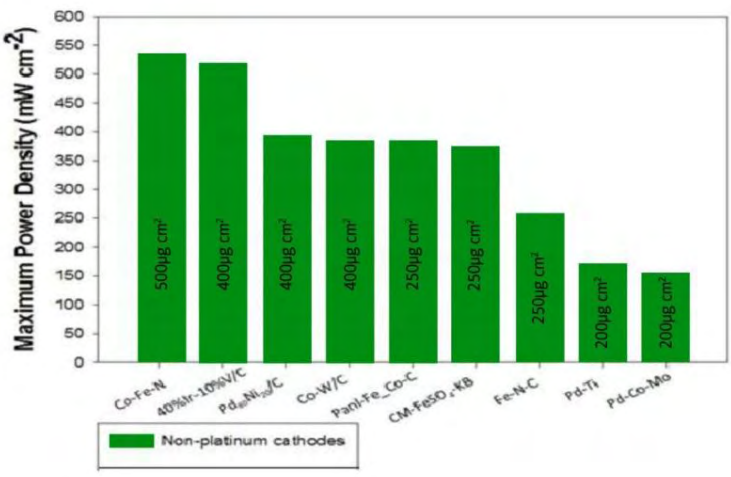

Figure 2.12.H_2-PEMFC operation results using non-platinum cathodes and platinum based anodes: maximum fuel cell power density (mW cm^{-2}) dependency on anode's platinum loading (μg cm^{-2})[4].

In the case that polyaniline [42] was used as carbon and nitrogen precursor, the cell maximum power density reached the value of 380 mW cm^{-2}, the anode's Pt loading was 250 μg cm^{-2}. In a general overview of fig.4.7, comparison of the performances exhibited by Pt catalysts, the transition metals (binary and ternary) carbides, nitrides and oxynitrides exhibited remarkably equal or slightly better performance with the same loading of metal. The most common examined binary and ternary alloys are Pd-Ti [43] which gave a value of about 170 mW cm^{-2}, Pd-Ni [53] which reaches the value of 390 mW cm^{-2} and Pd-Co-Mo [45] with a maximum power density of 150 mW cm^{-2}. The cobalt tungsten Co-W/C treated by ammonia [47] obtained performance of 382 mW cm^{-2} (anode Pt loading: 400 μg cm^{-2}) obtained performance of 382 mW cm^{-2} (anode Pt loading: 400 μg cm^{-2}). According to Zelenay et al.[46] using cathode catalyst cyanide as a nitrogen source, H_2-PEMFC exhibited a maximum power density of 370 mW cm^{-2}. A highly ordered Pt-free Fe-N-C catalyst is synthetized by Tang et al. [54] achieving maximum power of the cell 252 mW cm^{-2}.

CHAPTER 3

3. EXPERIMENTAL SECTION AND TECHNIQUES

In Chapter 3 the experimental techniques and their main principles that were used for the physicochemical and electrochemical characterization of the studied electrocatalysts are described. Additionally, before the experimental techniques the electrocatalysts' preparation method is referred. The electrocatalysts were prepared by a modified microwave assisted polyol method. Their physicochemical characterization was conducted by the techniques of Transmitting Electrode Microscopy (TEM) and X-Ray Diffraction (XRD). Their electrochemical characterization towards hydrogen and oxygen electrooxidation was conducted by the Cyclic Voltammetry, Chronoamperometry and Rotating Disk methods.

3.1. Experimental apparatus

3.2. Physicochemical characterization

The two physicochemical techniques used to characterize catalysts during this work, XRD and TEM, measure the structure and/or chemical composition of catalysts extending below the catalytic surface. The composition of the surface is usually different from that of the bulk. It is on these surfaces that the active sites exist and where chemisorption, chemical reaction, and desorption take place.

3.2.1. Transmission electron microscopy (TEM)

TEM investigations were carried out on a FEI/Philips CM12 EDX microscope to determine the size and surface morphology of the catalyst particles. It operates at 12 kW and is equipped with LaB6. Before the measurements, the catalysts were uniformly dispersed in ethanol solution using an ultrasonic water bath and then few drops of this solution were deposited on a copper grid.

Figure 3.1. FEI/ PhilipsCM12 EDXmicroscope.

3.2.1.1. Historical backround

The *resolution* ρ of a microscope is defined as the distance between two details in a just small distance from one another. It can be calculated using the Abbe theory of images formation for optic systems. For incoherent light or electron beam:

$$\rho = \frac{0.61\lambda}{sin\alpha} \quad (1)$$

Where λ is the wavelength of the light and αthe maximum angle between incident and deflected beam in the limit of the lens aberrations. In 1923, De Broglie showed that all particles have an associated wavelength linked to their momentum: where *m* and *v* are

the relativist mass and velocity respectively and *h* the Plank's constant.[55] In 1927, Hans Bush showed that a magnetic coil can focus an electron beam in the same way that a glass lens for light. Five years later, a first image with a TEM was obtained by Ernst Ruska and Max Knoll. In a TEM, the electrons are accelerated at high voltage (100-1000 kV) to a velocity approaching the speed of light (0.6-0.9 *c*); they must therefore be considered as relativistic particles. The associated wavelength is five orders of magnitude smaller than the light wavelength (0.04-0.008 Å). Nevertheless, the magnetic lens aberrations limit the convergence angle of the electron beam to 0.5° (instead of 70° for the glass lens used in optics), and reduce the TEM resolution to the Å order. This resolution enables material imaging and structure determination at the atomic level. In the 1950s, Raymond Castaing developed an electron probe and X-ray detector for the chemical analyses. A modified version of his technique, the energy dispersive spectrometry EDS is nowadays usually added to the TEM.

3.2.1.2. Principles of operation

Theoretically, the maximum resolution, *d*, that one can obtain with a light microscope has been limited by the wavelength of the photons that are being used to probe the sample, λ and the numerical aperture of the system:

$$d = \frac{\lambda}{2n\sin\theta} \qquad (2)$$

The previous equation is Bragg's equation where θ is the incident and reflected angle; the angle between the incident ray and the reflected angle is called diffraction angle and it is equal to 2θ [55].

Mid twentieth century researchers' guessed methods for getting around the constraints of the generally huge wavelength of obvious light (wavelengths of 400–700 nanometers) by utilizing electrons. Like all matter, electrons have both wave and molecule properties (as estimated by Louis-Victor de Broglie), and their wave-like properties imply that a light emission can be made to carry on like a light emission radiation. The wavelength of electrons is identified with their motor vitality by means of the de Broglie mathematical statement. An extra redress must be made to record for relativistic impacts, as in TEM an electron's speed methodologies the pace of light:

$$\lambda \approx \frac{h}{\left[2\, m_0\, E\, \left(1 + \frac{E}{2 m_0 c^2}\right)^{1/2}\right]} \qquad (3)$$

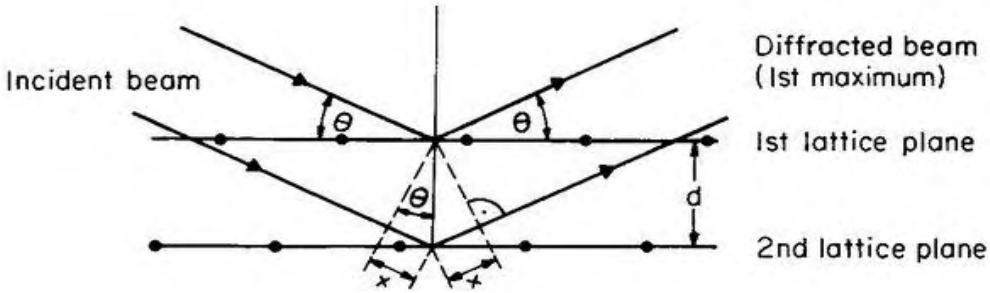

Figure 3.2. Bragg's diffraction[3].

Where *h* is Planck's constant, m_0 is the rest mass of an electron and *E* is the energy of the accelerated electron. Electrons are generally produced in an electron magnifying lens by a methodology known as thermionic discharge from a fiber, normally tungsten, in the same way as a light, or then again by field electron emanation. The electrons are then quickened by an electric potential (measured in volts) and concentrated by electrostatic and electromagnetic lenses onto the specimen. The transmitted shaft contains data about electron thickness, stage and periodicity; this bar is utilized to structure a picture.

A TEM analysis system consists of the three following main parts:

- Source formation: from the top down, the TEM consists of an emission source, which may be a tungsten filament, or a lanthanum hexaboride (LaB_6) source. For tungsten, this will be of the form of either a hairpin-style filament, or a small spike-shaped filament[3]. LaB_6 sources utilize small single crystals. By connecting this gun to a high voltage source (typically ~100–300 kV) the gun will, given sufficient current, begin to emit electrons either by thermionic or field electron emission into the vacuum. This extraction is usually aided by the use of a Wehnelt cylinder. Once extracted, the upper lenses of the TEM allow for the formation of the electron probe to the desired size and location for later interaction with the sample. Manipulation of the electron beam is performed using two physical effects. The interaction of electrons with a magnetic field will cause electrons to move according to the right hand rule, thus allowing for electromagnets to manipulate the electron beam. The use of magnetic fields allows for the formation of a magnetic lens of variable focusing power, the lens shape originating due to the distribution of magnetic flux.

Additionally, electrostatic fields can cause the electrons to be deflected through a constant angle. Coupling of two deflections in opposing directions with a small intermediate gap allows for the formation of a shift in the beam path, this being used in TEM for beam shifting, subsequently this is extremely important to STEM. From these two effects, as well as the use of an electron imaging system, sufficient control over the beam path is possible for TEM operation. The optical configuration of a TEM can be rapidly changed, unlike that for an optical microscope, as lenses in the beam path can be enabled, have their strength changed, or be disabled entirely simply via rapid electrical switching, the speed of which is limited by effects such as the magnetic hysteresis of the lenses.

- Optics: The lenses of a TEM consider bar meeting, with the point of union as a variable parameter, giving the TEM the capacity to change amplification essentially by adjusting the measure of current that moves through the curl, quadrupole or hexapole lenses. The quadrupole lens is a game plan of electromagnetic loops at the vertices of the square, empowering the era of a lensing attractive fields, the hexapole arrangement just improves the lens symmetry by utilizing six, instead of four curls. Commonly a TEM comprises of three phases of lensing. The stages are the condenser lenses, the goal lenses, and the projector lenses. The condenser lenses are in charge of essential bar arrangement, whilst the target lenses center the bar that gets through the specimen itself. The projector lenses are utilized to grow the bar onto the phosphor screen or other imaging gadget, for example, film. The amplification of the TEM is because of the degree of the separations between the example and the goal lens' picture plane [3].
- Display: Imaging frameworks in a TEM comprise of a phosphor screen, which may be made of fine (10–100 μm) particulate zinc sulfide, for direct perception by the administrator. Alternatively, a picture recording framework, for example, film based or doped YAG screen coupled CCDs. Ordinarily these gadgets can be uprooted or embedded into the shaft way by the administrator as needed.

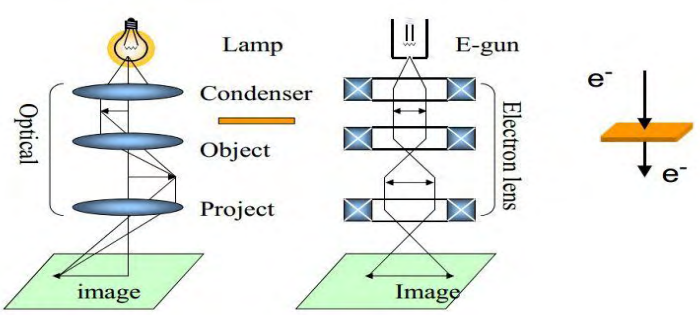

Figure 3.3. Schematic representations of components of a TEM[3].

3.2.2. X-Ray diffraction technique

X-ray powder diffraction (XRD) is one of the most powerful techniques for qualitative and quantitative analysis of crystalline compounds. This provides information that cannot be obtained with any other way. The information that can be obtained includes types and nature of present crystalline phases, structural make-up of phases, degree of crystallinity and the amount of amorphous content, microstrain & size and orientation of crystallites [56].

3.2.2.1. Principle of operation

When a material (sample) is irradiated with a parallel beam of monochromatic X-rays, the atomic lattice of the sample acts as a three dimensional diffraction grating causing the X-ray beam to be diffracted to specific angles. The diffraction pattern, that includes position (angles) and intensities of the diffracted beam, provides much information about the sample, which is discussed below:

- Angles are utilized to ascertain the interplanar nuclear spacings (dspacings). Since each crystalline material will give a trademark diffraction design and can go about as an exceptional 'finger impression', the position (d) and power (I) data are utilized to recognize the sort of material by contrasting them and examples for more than 80,000 information entrances in the International Powder Diffraction File (PDF) database, went along by the Joint Committee for Powder Diffraction Standards (JCPDS). By this system, recognizable proof of any crystalline mixes, even in a complex example, can be made.
- The position (d) of diffracted peaks also provides information about how the atoms are arranged within the crystalline compound (unit cell size or lattice parameter). The intensity information is used to assess the type and nature of atoms. Determination of lattice parameter helps understand extent of solid solution (complete or partial substitution of one element for another, as in some alloys) in a sample.

- Width of the diffracted peaks is used to determine crystallite size and micro-strain in the sample.
- The ‘d’ and ‘I’ from a phase can also be used to quantitatively estimate the amount of that phase in a multi-component mixture.

The quantitative analysis is one of the important advantages of X-ray diffraction technique. Several methods have been proposed and successfully used to quantify crystalline phases in mixtures. They include external standard methods, the reference-intensity-ratio (RIR) method, chemical methods and the whole pattern fitting Rietveld method. Of the available methods, the Rietveld method is probably the most accurate and reliable method. It is a whole-pattern fitting least squares refinement technique and has been successfully used for quantification and characterization of inorganic and organic compounds. It has also been used for crystal structure refinement, to determine size and strain of crystallites[56].

Figure 3.4. Fitting of a X-ray diffraction peak[56].

3.3. Methods for catalysts’ characterization

3.3.1. Electrochemical methods for evaluating catalytic activity

The electrocatalytic activity of catalysts before their use in fuel cells has been evaluated by electrochemicals methods. Two types of electrochemical tests are employed in this study. The first test is a cyclic voltammetry test (CV) and the second is the rotating disk electrode (RDE). An electrochemical reaction includes at least the following steps:

- Reactants transport to the electrode surface;
- Reactants adsorbed onto the electrode surface;
- Charge transfer through either oxidation or reduction on the surface of the electrode;
- Products transport from the electrode surface.

The aim of the electrochemical characterizations is to determine the details of these steps.

Electrochemical characterization is performed in different types of electrochemical cells. The most used three types of cells are: conventional 3-electrode cells, half-cells and single cells. In these cells the entity to be characterized, forms the working electrode and its potential in a way that the current flowing through it, is controlled or monitored. The sole interest of the analysis is what happens on the working electrode. The working electrode and another electrode, called the counter electrode, form a circuit, and the current flowing through this circuit will cause some reaction on the counter electrode as well. However, the investigation has no interest in what happens on the counter electrode, except that the reaction occurring on it should not interfere with the working electrode[57].

In order to minimize the impact of the solution (or the electrolyte) resistance on the potential of the working electrode, a reference electrode is often used to form another circuit with the working electrode. Ideally, this electrode is non-polarizable and maintains a stable potential. There is high input impedance in the voltage measurement equipment, which makes the current flowing in this circuit very small. Therefore, the impact of the uncompensated electrolyte resistance on the potential of the working electrode is minimized. All electrochemical techniques involve the use of electricity as either an input or an output signal. The function of an electrochemical instrument is to generate an input electrical signal and to measure the corresponding output electrical signal. The input signals can be a pre-programmed function of time, while the output signals often change with time. The signals are typically voltage, current, and charge. Charge is the integration of current with time. The input electrical signal causes the electrochemical reactions at the working and the counter electrodes. The rate of the reactions is controlled by the amplitude of the input signal and is represented by the amplitude of the output signal.

3.3.2. Cyclic Voltammetry

3.3.2.1. Basic principles

Cyclic voltammetry refers to cycling the potential between a low and high potential value and recording the current in the potential cycling region. The resulting potential versus current plot is called a voltammogram. The sweeping of the potential is carried out

linearly, and the sweeping rate can be controlled in a wide range. Most studies are carried out with a potential scanning rate between 1 and 1000 mV s^{-1}. The key things that voltammogram offers are:

- Peak current (i_d). It depends linearly on the analyte concentration and on square root of scan rate. If the graph i_p vs $v^{1/2}$ is linear, we can say that the process is controlled by mass transfer phenomena of electro-active specie towards the electrodic surface through a concentration gradient. A feature of reversible system is that: $i_{pc}=i_{pa}$;
- Peak potential (E_p). If the electronic transfer rate is high, e_p is independent from the scan rate. If the coefficients of oxidized and reduced species are similar, the medium value between anodic peak potential (E_{pa}) and cathodic peak potential (E_{pc}) corresponds to E° (which depends on the nature of electrolytes present in the solution)[58].

$$\mathrm{E_{midpoint}} = \frac{(\mathrm{E_{pa}}+\mathrm{E_{pc}})}{2} = E° + \frac{RT}{nF}\ln\frac{(D_{RED})^{1/2}}{(D_{OX})^{1/2}} \quad (4)$$

The separation of peaks is given by:

$$\Delta E_p = |E_{pa} - E_{pc}| = 2{,}3\,\frac{RT}{nF} = (\frac{59}{n})mV \text{ and } 298\ \mathrm{K} \quad (5)$$

In a voltammogram we rarely obtain the result of 59 mV. To achieve this value and to assure that the electrode behavior is nernstian, it is necessary to use low scan rate. When the flowing current is low, the electronic transfer has more possibilities to be faster than mass transfer phenomena.

Before the scanning starts, the working electrode is usually held at a potential that does not cause any electrochemical reactions. After the start of the scanning, the potential goes higher (or lower), and when it becomes high (or low) enough to cause the oxidation (or reduction) of an electrochemically active species, an anodic (or cathodic) current appears. The anodic (or cathodic) current increases as the potential increases (or decreases) because the reaction kinetics becomes faster. When the potential reaches the standard potential E°, the concentrations, of the oxidized and the reduced forms of the electrochemically active species, become equal on the surface of the electrode. The highest anodic (or cathodic) current is reached when the potential reaches a value at which all the reduced (or oxidized) form of the electrochemically active species at the

electrode surface is consumed. The highest current is achieved at this moment because the mass transport rate of the electrochemically active species reaches a maximum rate, driven by the (largest) concentration gradient between the bulk concentration of the electrochemically active species and the surface concentration of this species. When the potential goes higher (or lower) beyond this point, the current starts to decline because the double-layer thickness increases, resulting in a less steep concentration gradient of the electrochemically active species [58]. Therefore, an anodic (or a cathodic) peak develops. When the potential reaches the set high (or low) limit, it reverses direction and scans towards the set low (or high) limit. During this reversed potential scan the oxidized (or reduced) form of the electrochemically active species reacts and develops a cathodic (or anodic) peak. The cathodic (anodic) peak is located at a slightly lower (higher) potential than the anodic (cathodic) peak. The cathodic and anodic peaks are of equal height (or, more accurately, equal area), unless there are complications caused by some side chemical or electrochemical processes. The above electrode steps can also be complicated by:

- the applied voltage on the electrode;
- the reactivity of the species;
- the nature of the electrode surface;
- The structure of the interfacial region over which the electron transfer occurs.

If the electrochemical reactions are thermodynamically reversible, the positions (voltage) of the cathodic or anodic peaks do not change with the potential scan rate (v) and the peak height is proportional to the square root of the potential scan rate, $v^{1/2}$, according to the Randles-Sevcik equation:

$$i_p = 2.69\, x\, 10^5\, n^{3/2}\, A\, Do^{1/2}\, v^{1/2}\, Co$$

Where i_p is the peak current (in amperes), n is the number of electrons per reactant molecule, A is the electrode area (cm^2), v is the potential scan rate ($V\ s^{-1}$), D is the diffusion coefficient ($cm^2\ s^{-1}$), and C is the bulk concentration of the reactant ($mol\ cm^{-3}$).

The addition of electrons to an oxidized reactant is termed reduction and oxidation is a process involving the removal of electrons:

$$\text{Oxidized species (A)} + ze^- \rightarrow \text{Reduced Species (B)}$$

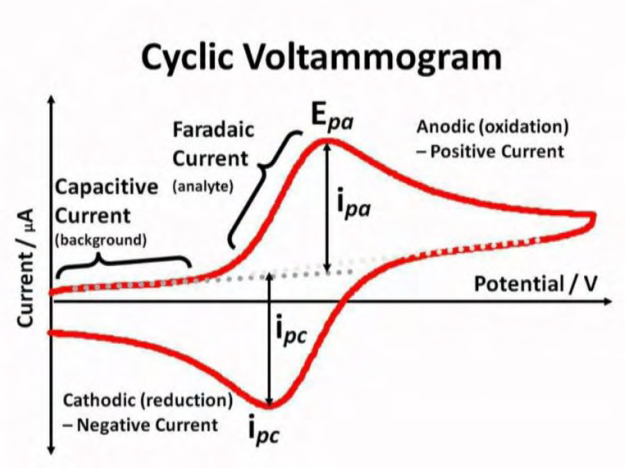

Figure 3.5. A typical cyclic voltammogram for a reversible reaction [58].

More precisely, the overall conversion of reactant A into product B must occur in a minimum of three steps:

Mass transfer

$$A_{solution} \text{----------} \rightarrow A_{electrode}$$

Electron transfer

$$A_{electrode} \text{----------} \rightarrow B_{electrode}$$

Mass transfer

$$B_{electrode} \text{----------} \rightarrow B_{solution}$$

Both processes (A to B and B to A) involve charge transfer. During polarization, measured currents produced by oxidation or reduction of electro-active species will be limited by one of the following rate determining steps:

1. The transfer of electrons at the electrode/electrolyte interface (charge transfer controlled current).

2. The movement of reactants or products at distances close to the electrode (mass transport controlled current).

3. A combination of the both above-mentioned occasions (mixed control current).

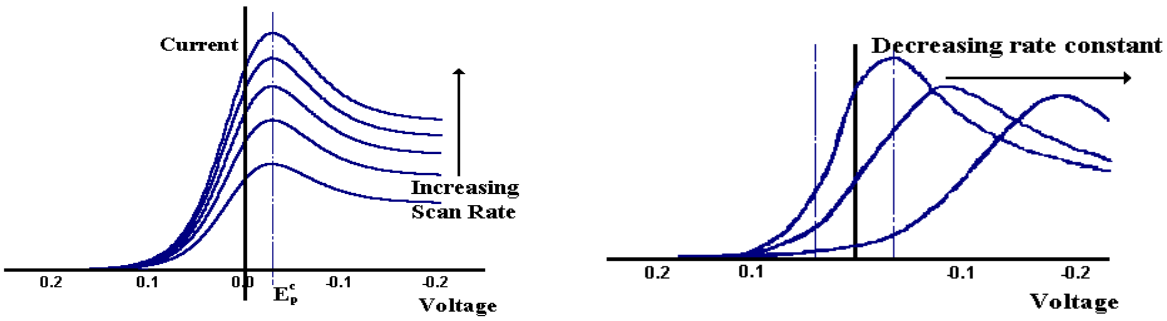

Figure 3.6. Mass transport controlled current and charge transfer controlled current.

The rate of conversion of the reactant in the bulk solution into product must always be determined by the slowest of these three steps. The rate of charge transfer between an electrode material and the electro-active species is related to how fast the substrate material can accept or give up electrons. This kinetic behavior of an electrode will depend on its surface “activity”. When dealing with the movement of charge, a simple way to improve the rate of reaction is to increase the potential difference (the applied energy). Then, catalytic activities accelerate without the required addition of extra energy. Generally in voltammetric analysis experiments are carried out in diffusive conditions: in a way that the current due to electro-active species is of the diffusive type, this approximation allows us to neglect the migration phenomena in calculation. To make this possible we need the presence of a support no electro-active electrolyte with a higher concentration than the other species. We need that the solution is quiescent.

3.3.2.2. Instrumental apparatus

During the experiments, gases were fed through the mass flow meters as it is shown in Fig.3.7.

Figure 3.7. Instrumental apparatus used in the experiment with a focus on moisture saturators and mass flow meters.

The analysis section is constituted by a galvanostatic/ potentiostatic system that allows measurements and tests of current and potential on the cell.

Figure 3.8. Electrochemical station AMEL 7050.

During our experiments, the electrochemical station AMEL 7050 has been used as an instrument able to function as a potentiometer, potentiostat and galvanostat. We have to mention its characteristics:

Table 3.1. Characteristics of AMEL 7050 electrochemical station.

Characteristics	*Values*
Potential range [V]	0 ± 45
Potential resolution [μV]	200
Current range [A]	0 ± 4
Current resolution [fA]	200
Accuracy [%]	0,2
Sampling rate [analysis/sec]	$1 \div 100$
Temperature resolution [°C]	0,1
Working electrode	1

This instrument is connected to three electrode system (cyclic voltammtery and rotating electrode techniques) and the data were recorded on computer automatically through the software Corrware.

The instrument used to perform cyclic voltammetry and potential step experiments is a potentiostat, which controls the voltage and measures the current. The potentiostat maintains the potential of the working electrode at a desired value with respect to the potential of the reference electrode. The current flows between the working and the counter electrodes in response to the potential of the working electrode.

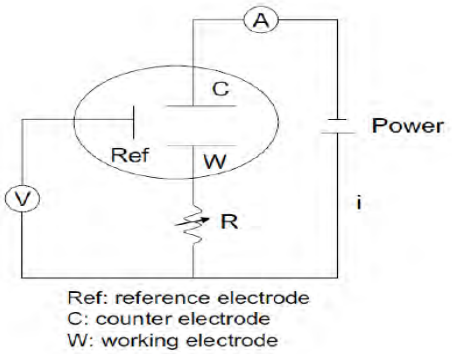

Figure 3.9. Illustration of the basic circuit of a potentiostat.

A resistance in the electric circuit is used to adjust and maintain the potential of the working electrode. A potentiostat measures the voltage difference between the reference and the working electrodes. A potentiostat has extremely high input impedance so that the input current is nearly zero, which enables the reference electrode to keep a constant potential. The current passing through the working and the counter electrodes is determined by measuring the voltage drop through a known resistor according to Ohm's law. When the electronic circuit is slightly modified so that the current is controlled and the corresponding potential of the working electrode is measured, it becomes a galvanostat.

3.3.3. Rotating disk electrode technique (RDE)

3.3.3.1. Basic principles

Hydrodynamic devices use convection to enhance the rate of mass transport to the electrode and can offer advantages over techniques which operate in stagnant solution. The addition of convection to the cell usually results in increased current and sensitivity in comparison to the voltammetric measurements performed in a stagnant solution. Also the introduction of convection (usually in a manner that is predictable) helps to remove the small random contribution from natural convection which can complicate measurements performed in stagnant solution. Finally, it is possible to vary the rate of reaction at the electrode surface by altering the convection rate in the solution and this can be usefully exploited in mechanistic analysis and electroanalytical applications. There are two main approaches of introducing convection into the electrochemical cell. First the electrode can be held in a fixed position and solution is flowed over the surface by an applied force (usually a pressure). Second the electrode can be designed to move which acts to mix the solution via convection. The introduced (forced) convection is generally made to be considerably stronger than any natural convection processes and therefore the influence of natural convection becomes insignificant on the electrochemical reaction. To allow quantitative analysis it is vital that the forced convection introduced to the cell is predictable. The cell and experimental conditions are therefore designed so that the solution flow within the cell becomes laminar.

3.3.3.2. Instrumental apparatus

In this apparatus, solution is brought to the surface by a rotating disk electrode, with the working electrode surface area in A= 0.07 cm^2. As reference electrode a saturated calomel electrode is used (Saturated Calomel electrode, SCE), while the platinum electrode is used as the auxiliary electrode. The measurements were taken with the particular electrochemical devices:

1. an electrochemical station AMEL 7050 & AMEL 5000 and
2. a rotating disk electrode system (AMEL RDE Radiometer system CTV101).

The rotating disk electrode consists of a cylindrical metal rod embedded within a larger cylindrical plastic (usually Teflon) holder. The electrode is cut and well-polished along with the holder, so that only the bottom end of the metal roll comes into contact with the solution.

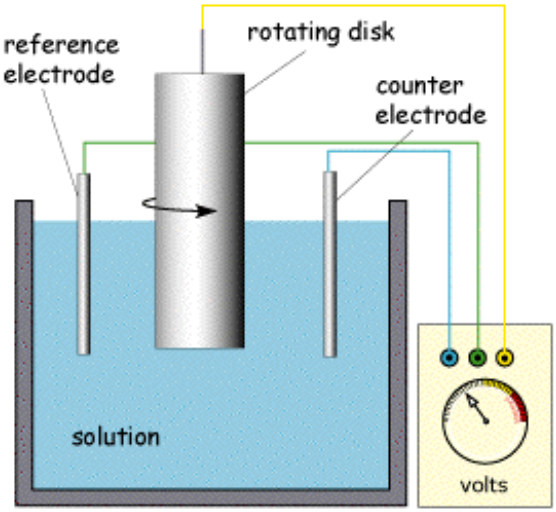

Figure 3.10. Rotating disk electrode equipment [59].

The main characteristic of a rotating disk electrode is that the mass transfer rate at the surface is uniform. This in any case is not self-evident, since we know that the linear velocity of the points on the surface increases with the distance from the center of rotation.

Moreover, another important property of a rotating disk electrode is that the flow of the solution around the electrode is laminar even at high speeds. The figure below shows the type of flow profile that is developed when a circular object is rotated in solution and how this brings fresh reactant to the surface[59].

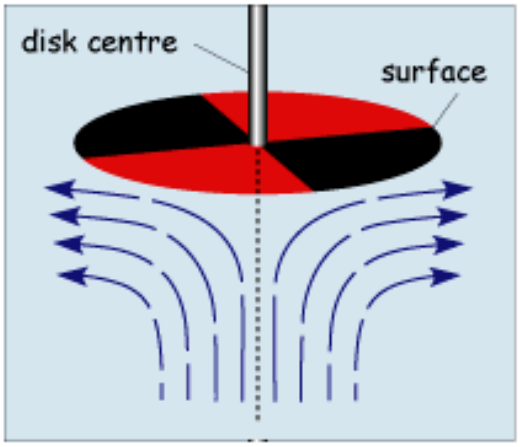

Figure 3.11. Scheme of the flow on working electrode surface [59].

The act of rotation drags material to the electrode surface where it can react. Providing that the rotation speed is kept within the limits that laminar flow is maintained then the mass transport equation is given by:

$$\frac{\partial[C]}{\partial t} = D_c \frac{\partial^2[C]}{\partial x^2} - v_x \frac{\partial[C]}{\partial x} \qquad (7)$$

Where the x dimension is the distance onto the electrode surface. It is apparent that the mass transport equation is now dominated by both diffusion and convection and both these terms effect the concentration of reagent close to the electrode surface. The convection term does not affect the reaction much, so it will be ignored in the experimental part. Therefore to predict the current for this type of electrode we must solve this subject to the reactions occurring at the electrode[59].

A typical voltammetric measurement used with the rotating disc and other hydrodynamic systems is linear sweep voltammetry.

The Figure below shows a set of current voltage curves recorded for a reversible on electron transfer reaction and different rotation speeds.

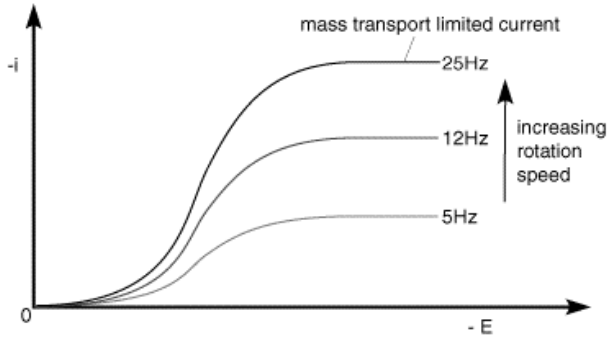

Figure 3.12. Linear sweeping voltammetric measurements with RDE [59].

As the rotation speed is increased the distance that material can diffuse from the surface before being removed by convection is decreased. This results in a higher flux of material to the surface at higher rotation speeds. The mass transport limited current arises from the fact that the system reaches a steady state and so the current reaches a plateau once the equilibrium at the surface is driven to the products side[59].

The Levich Equation models the diffusion and solution flow conditions around a Rotating disk electrode (RDE). It can be used to predict the current observed at an RDE; in particular, the Levich equation gives the height of the sigmoidal wave observed in rotating disk voltammetry[59].

$$i_d = 0{,}62\, n\, F\, D^{2/3} \nu^{-1/6} C_0 \omega^{1/2} \qquad (8)$$

Where: id is the limiting diffusion current, n is the number of electrons transferred in the half- reaction(oxidation of hydrogen or reduction of oxygen), F is the Faraday constant (96485 C mol^{-1}), D is the diffusion coefficient, ν is the kinematic viscosity of the electrolyte,$C$is the analyte concentration, ω is the angular rotation rate of the electrode.

To calculate the kinetic current density the Koutechy-Levich equation is used:

$$\frac{1}{i} = \frac{1}{i_k} + \frac{1}{i_d} \qquad (9)$$

Where i is the recorded current in this potential and i_k is the kinetic current density.

Also for the RDE measurements was used the electrochemical station that was described above[32, 59].

CHAPTER 4

4. CHARACTERIZATION OF PdxRhy BASED ANODES AND CATHODES FOR HYDROGEN OXIDATION AND OXYGEN REDUCTION REACTIONS

In Chapter 4, the catalyst preparation is analyzed and also the mechanical dissolution of two bimetallic catalysts is introduced. In the present chapter carbon Vulcan XC-72R supported PdxRhx (x=1:1, 3:1, 1:3) nanoparticles have been prepared by a modified pulse microwave assisted polyol method and have been studied for hydrogen electrooxidation in sulphuric acid media. The PdxRhx/C electrocatalysts have been characterized by X-ray diffraction (XRD), Transmission Electron Microscopy (TEM), Cyclic Voltammetry (CV), Rotating Disk Electrode (RDE) and Chronoamperometric measurements (CA). The effects of the concentration of electrolyte and PdxRhx as well as of temperature on the activity of hydrogen electrooxidation have been investigated. According to the results, the electro-catalytic activity towards hydrogen electrooxidation of the investigated catalysts has the following order: Pd/C < Pd3Rh/C < Rh/C < PdRh/C < PdRh3/C.

4.1. Experimental procedure

4.1.1. Catalyst preparation

The catalytic paste was prepared according to the following procedure: 2.0 mg of catalyst were dissolved in 1.8 mL of ethanol and 0.2 mL Nafion ionomer stirring in an ultrasonic bath for 40 minutes, so as to create a uniform solution of black color. Then 4μL of this solution by means of micro- syringe were deposited on the surface of the working electrode. With the help of infrared radiation, the solvent evaporates and a thin catalytic film is formed on the surface of the working electrode (A = 0.07cm^2). The catalyst ink was then quantitatively transferred onto the surface of the GC electrode and dried to obtain a catalyst thin film. The estimated amount of catalyst loading on the glassy carbon electrode surface was maintained to be 0.011mg cm^{-2}. All the experiments were conducted using H_2SO_4 (Carlo Erba, 96%) electrolyte solution at 25°C, 40°C and 50°C [60].

4.1.2. Physicochemical measurements of Pd_xRh_x

XRD patterns of the as-prepared electrocatalysts are shown in Fig. 4.2. The first peak at 25° is associated with the Vulcan XC-72 support material for all the five samples [61].

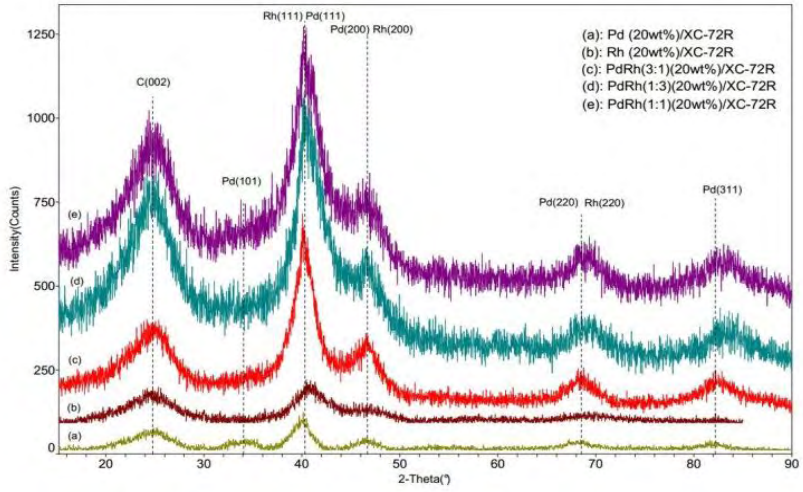

Figure 4.1. X-ray diffraction patterns of (a) Pd/XC-72R, (b) Rh/XC-72R, (c) PdRh(3:1)/XC-72R, (d) PdRh(1:3)/XC-72R and PdRh(1:1)/XC-72R bimetallic catalysts prepared with polyol reduction.

The other four main characteristic diffraction peaks at ca. 40°, 48°, 68° and 83° belonging to the face-centered cubic crystalline Pd (1 1 1), (2 0 0), (2 2 0), (3 1 1), respectively. The (1 1 1) plane has the largest intensity among others planes, which becomes more with respect to the corresponding peak in the Pd/XC-72 and Rh/XC-72 catalyst, indicating the effect of increased amounts of Rh in the Pd_xRh_x bimetallic

catalysts. Moreover as the palladium ratio increases the Pd (1 1 1) peak position slightly shifts to more positive angles 2θ values, revealing decreased lattice parameters and a high level of alloying [60].

TEM images of the Pd/Vulcan XC-72, Rh/Vulcan XC-72 and PdxRhx catalysts are shown in Fig. 4.2, in order to examine the surface morphology of the prepared electrocatalysts. The image of Pd/C in Fig. 4.2.(A) shows that Pd nanoparticles are well dispersed on the support.

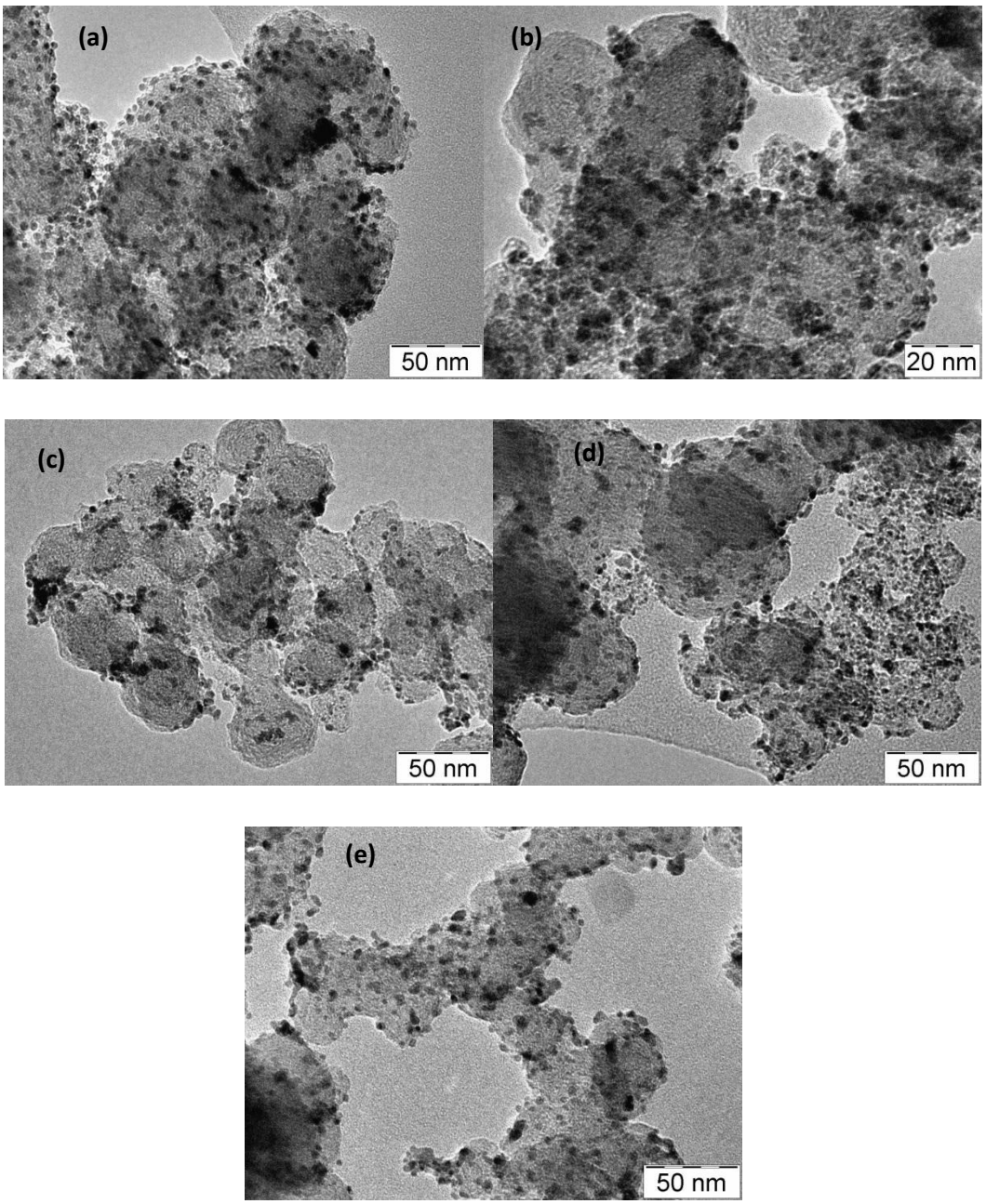

Figure 4.2. TEM images of (a) Pd/C, (b) Rh/C, (c) PdRh(1:3), (d) PdRh(1:1), (e)PdRh(3:1).

4.2. Electrochemical analysis of Pd_xRh_x

4.2.1. Electrochemical active surface area-Cyclic voltammetry measurements

Cyclic voltammetry is probably the most widely used technique for the electrochemical characterization of the electrocatalysts. It is well known that the voltammogram recorded under given conditions is characteristic of the individual noble metal and it is an electrochemical 'fingerprint' of the investigated sample. The surface of noble metal alloy can be characterized by identifying the distinctive CV features associated with each component.

Fig.4.3 shows the voltammetric profiles of the as-prepared bimetallic films obtained in 0.5 M H_2SO_4 solution at the scan rate of 50 mV s^{-1}. CV was performed to determine the electrochemical surface area and to elucidate the adsorption properties of the catalyst [60] [61].

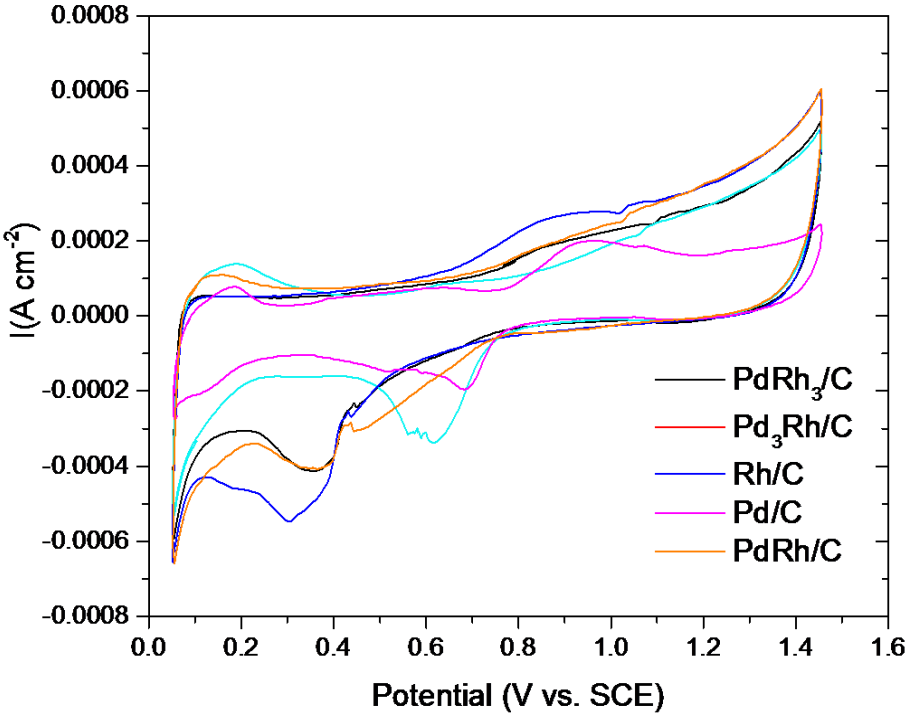

Figure 4.3. Cyclic voltammograms for Pd/Vulcan XC-72, PdRh(3:1)/Vulcan XC-72, PdRh(1:1)/Vulcan XC-72, PdRh(1:3)/Vulcan XC-72 and e) Rh/Vulcan XC-72 in 0.5 M H_2SO_4 de-oxygenated and saturated with H_e, the potential scan speed is 50 mV s^{-1}.

For a positive-going sweep the first peak (at 0 to ~0.15V versus SCE) represents hydrogen desorption region. The oxidation/reduction peaks corresponding to the formation of palladium oxide during the cathodic scan may be observed in at around 0,6 V (SCE). The redox peaks in the 0.8–1.2 V region corresponding to the formation and reduction of

surface Pd oxides (Pd–OH or PdOx species). It is known that the PdOx species at the metallic Pd surface is inactive toward oxygen reduction.

CV was employed to obtain the electrochemical active area of the different catalysts. The coulombic charge for hydrogen desorption (Q_H) was used to calculate the active Pd-based electrocatalysts surfaces of the electrodes. It is well known that this area of the aforementioned peak can be used to calculate the electrochemical surface area (ECSA) of the electrocatalysts and can be obtained by using the following Equation:

$$EASA\left[\frac{m^2}{g}\right] = charge[\mu C/cm^2]/420[\mu C/cm^2] \times Catalyst\ loading\ [mg\ /\ cm^2] \times 10$$

Where, integrated charge in the hydrogen adsorption peak area in the CV curves in Fig. 4.3 and the specific amount of electricity corresponding to the full coverage of the Pd surface by one monolayer of oxygen was taken as 420 μCcm^{-2}. In the case of Pd-based electrocatalysts the electrochemical active surface area (EASA) is calculated by determining the coulombic charge (Q) for the education of palladium oxide peak [60].

According to the results of the calculations, the ECSA are compiled in Table 4.1:

Table 4.1. Electrocatalytickinetic parameters on different electrodes in 0.5 mol L^{-1} H_2SO_4, at 25 ^{o}C, 50 mV s^{-1}.

Electrode 20%wt	Pd loading (μg cm^{-2})	Rh loading (μg cm^{-2})	ECSA ($m^2\ g^{-1}$)$_{Pd}$
Pd/ Vulcan XC-72	11	0	21
PdRh(3:1)/ Vulcan XC-72	8.3	2.7	22.5
PdRh(1:1)/Vulcan XC-72	5.6	5.4	27.0
PdRh(1:3)/Vulcan XC-72	2.8	8.2	29.5
Rh/ Vulcan XC-72	0	11	25.6

These results clearly demonstrate that wide range of ECSA is obtainable simply by changing the palladium loading. From Table 4.1 the catalyst of PdRh(1:1)/Vulcan XC-72 and PdRh(1:3)/Vulcan XC-72 have a higher electrochemical active surface area (27.0 m^2/g and 29.5 m^2/g at 25.5^{0}C, respectively) in comparison with the other two catalysts (22.5 and 25.6 m^2/g at 25.5^{0}C) because of the smaller particle size Pd, which has been deposited on the electrode surface.As it can be noticed, the electrochemical active surface area exhibits the following order: Pd/C < Pd3Rh/C < Rh/C < PdRh/C < PdRh3/C [61].

4.2.2. Hydrogen oxidation reaction measurements

The presented results show that all prepared catalysts have a high loading for the hydrogen oxidation reaction. Pd, which is comparable to Pt in the hydrogen oxidation reaction (HOR) activity, is employed as an anode catalyst. Figure 4.4 shows the HOR polarization curves on Pd_xRh_x in 0.5M H_2SO_4 at room temperature as a function of rotation rate, with well-defined hydrogen mass transport controlled current densities occurring at potentials above 0.05 V.

To determine the catalytic activity of the material, we adopted the Koutecky–Levich analysis, where the catalytic current is related to the rotational velocity of the RDE through the equation. It is generally accepted that the hydrogen electrode reaction on a metallic surface is verified through the elementary steps of Tafel, Heyrovsky, and Volmer.

$$H_2 + 2S \leftrightarrows 2H_{ad} \quad Tafel \qquad (1)$$

$$H_2 + S \leftrightarrows H_{ad} + H^+ + e^- \quad Heyrovsky \qquad (2)$$

$$H_{ad} \rightleftarrows H^+ + e^- + S \quad Volmer \qquad (3)$$

Where S represents a site on the electrode surface in which the reaction intermediate H_{ad} can be absorbed. The resolution of the kinetic mechanism of Tafel-Heyrovsky-Volmer implies that the hydrogen oxidation is verified under the simultaneous occurrence of both Tafel-Volmer and Heyrovsky-Volmer routes.

Table 4.2.Kinetic current densities (i_k) for Pd_xRh_x and their ratios in HOR.

Electrode 20%wt (metal loading)	Tafel slope (mV decade^{-1})	I_0 (mA cm^{-2})	i_k (@0.1V) (mA cm^{-2})
Pd/ Vulcan XC-72	80.0	0.32	3.0
PdRh(3:1)/ Vulcan XC-72	120.0	1.24	4.0
PdRh(1:1)/Vulcan XC-72	230.0	1.75	7.3
PdRh(1:3)/Vulcan XC-72	180.0	3.00	7.6
Rh/ Vulcan XC-72	210.0	2.58	6.0

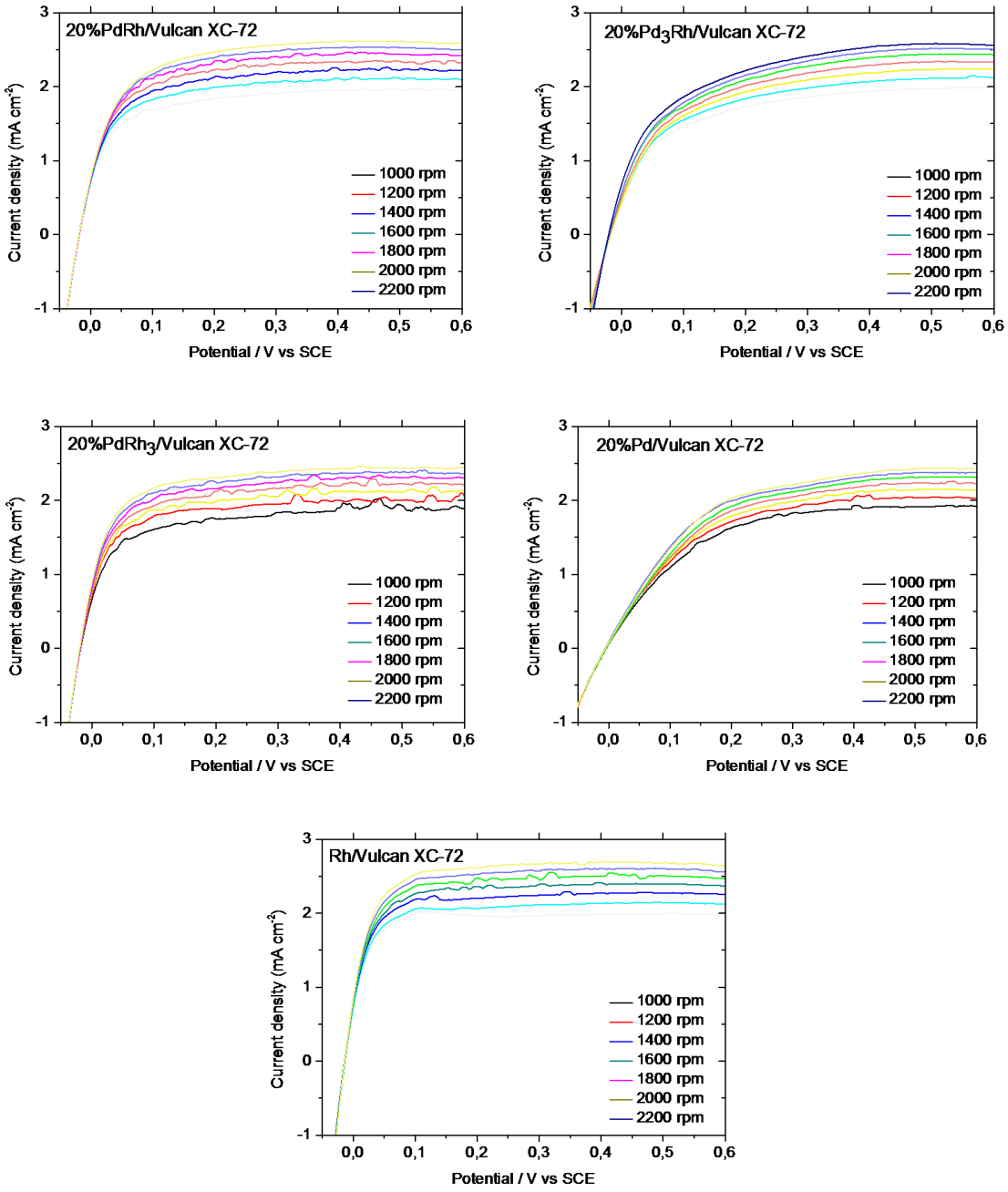

Figure 4.4.RDE curves in H_2-saturated 0.5 M H_2SO_4 at 5 mvs^{-1} for a)PdRh (1:1)/Vulcan XC-72, b)PdRh(3:1)/Vulcan XC-72, c)PdRh (1:3)/Vulcan XC-72, d) Pd/Vulcan XC-72 and e) Rh/Vulcan XC-72.

The measured total current density in RDE was composed of the kinetic current density (j_k) and diffusion limited current density (j_d) since the film resistance of Nafion is sufficiently small. Therefore, Koutecky–Levich equation is following as:

$$\frac{1}{i} = \frac{1}{i_k} + \frac{1}{i_d}$$

Where i is the experimental value of the current, i_k represents the kinetic current in the absence of mass transfer limitations and i_d is the diffusion-limited current. The later can be calculated according to the Levich equation:

$$i_d = 0.62nFD^{2/3}\nu^{-1/6}C\omega^{1/2}$$

Where n is the number of theoretically-transferred electrons (=2), F the Faraday constant (96485 C/mol), D the diffusion coefficient of H_2 in the H_2SO_4, v the kinematic viscosity of the electrolyte and C the H_2 concentration in the electrolyte of the dissolved-oxygen at an oxygen partial pressure of 1 bar ($1.26\ 10^{-6}$ mole cm^{-3});. The kinetic current density was graphically determined ($1/i$ vs. $1/\omega^{1/2}$ - Koutecky-Levich plots) [60].

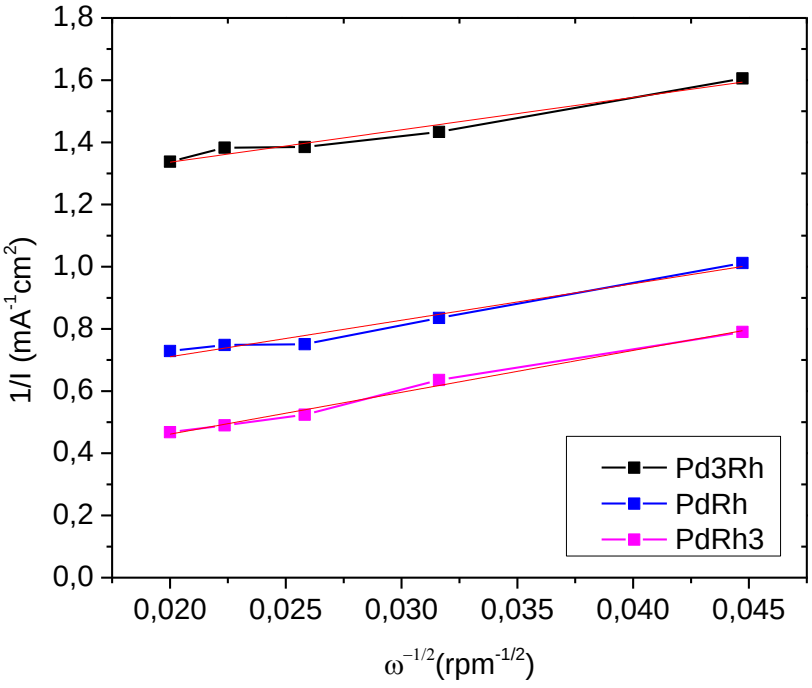

Figure 4.5. Koutecky-Levich plots for the hydrogen oxidation reaction.

The HOR/HER kinetic current densities (i_k) on Pd_xRh_x are shown in Fig. 4.6 which were obtained from correcting the polarization curves by the measured iR and the hydrogen mass transport in the HOR branch [61].

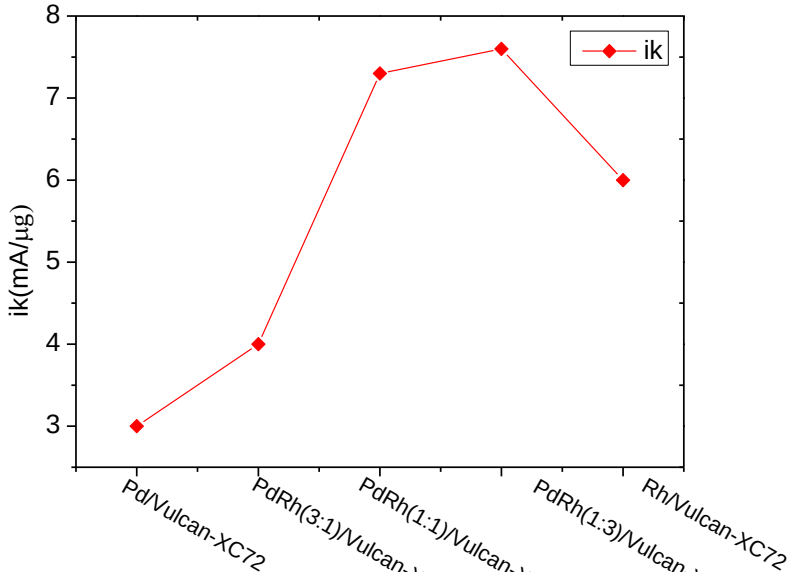

Figure 4.6. ik for Pd_xRh_x in hydrogen reduction.

In order to do further kinetic analysis the mass transfer corrected Tafel equation was adopted:

$$\log(i_k) = \log(i_o) + (\frac{anF}{2.303RT})\eta$$

From Tafel plot (logI vs. η) can be derived the exchange current density (i_0) value that gives relative rates of reaction at equilibrium being calculated from the intercept at y-axis at the region (20 to 50 mV vs. SCE).

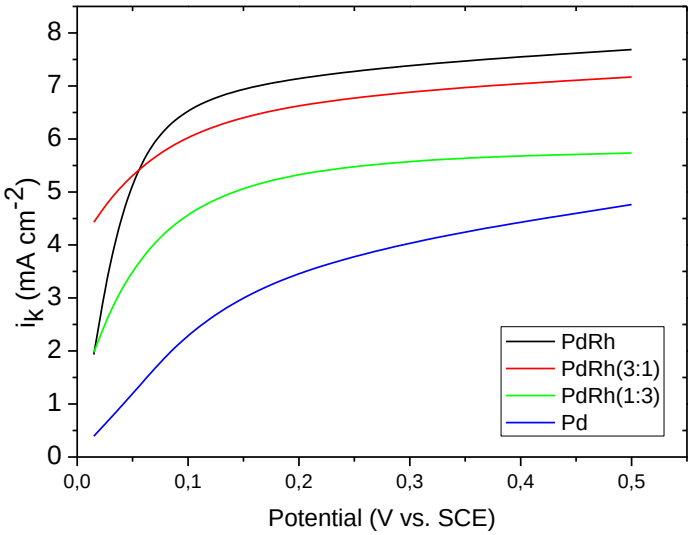

Figure 4.7. Tafel plots for the hydrogen oxidation reaction.

In Fig4.7, the calculated exchange current density is compared. It is found to has the following order: 20%PdRh (3:1)> 20%PdRh (1:1)> 20%PdRh (1:3) > 20%Pd respectively. In all cases Pd loading equals to 11 μgcm^{-2}.The increase of Rh loading seems to affect positively the electrocatalysts' behavior [61].

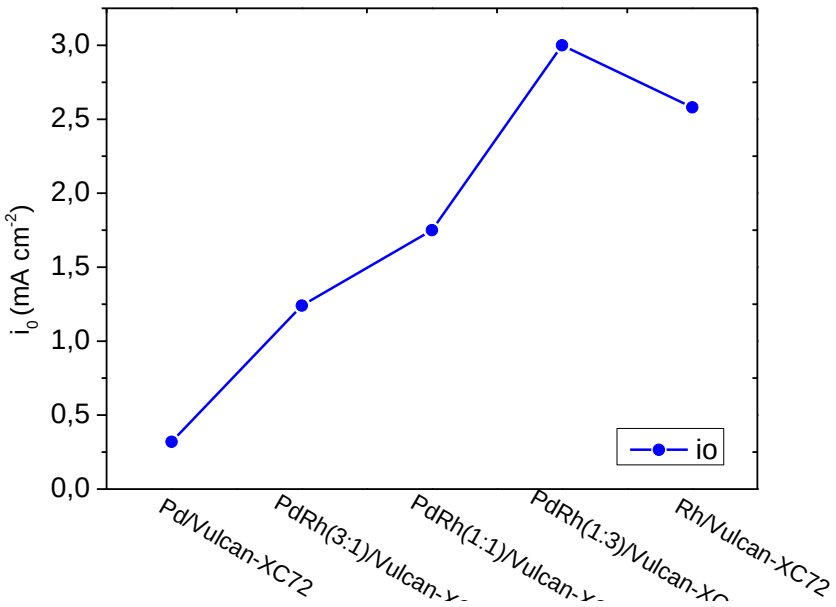

Figure 4.8. i_0 for Pd_xRh_x in hydrogen reduction.

In order to have a better understanding about the effect of Rh activity (to the kinetic and exchange current) of the examined electrocatalysts, Fig 4.8 is given. From this it can be derived that, the increase of the Rh loading strongly enhances the electrocatalytic activity of Pd towards HOR in terms of both exchange current and kinetic density densities. The increased electrocatalytic activity of PdRh bimetallic electrocatalysts could be attributed to their ability to adsorb more hydrogen than Pd [61].

4.2.3. Oxygen reduction reaction measurements

Figure 4.8 shows the ORR polarization curves on Pd_xRh_x , Pd_x and Rh_x in 0.5M H_2SO_4 at room temperature as a function of rotation rate, with well-defined hydrogen mass transport controlled current densities occurring at potentials above 0.05V .

We can observe from ORR curves in Fig.4.8 that while adding Rh to a Pd catalyst, this results in improving the catalyst's ORR activity. With Rh giving the highest current density, the ratio PdRh (3:1) follows and then the current density is lower in the ratios PdRh (1:1) and PdRh(1:3).

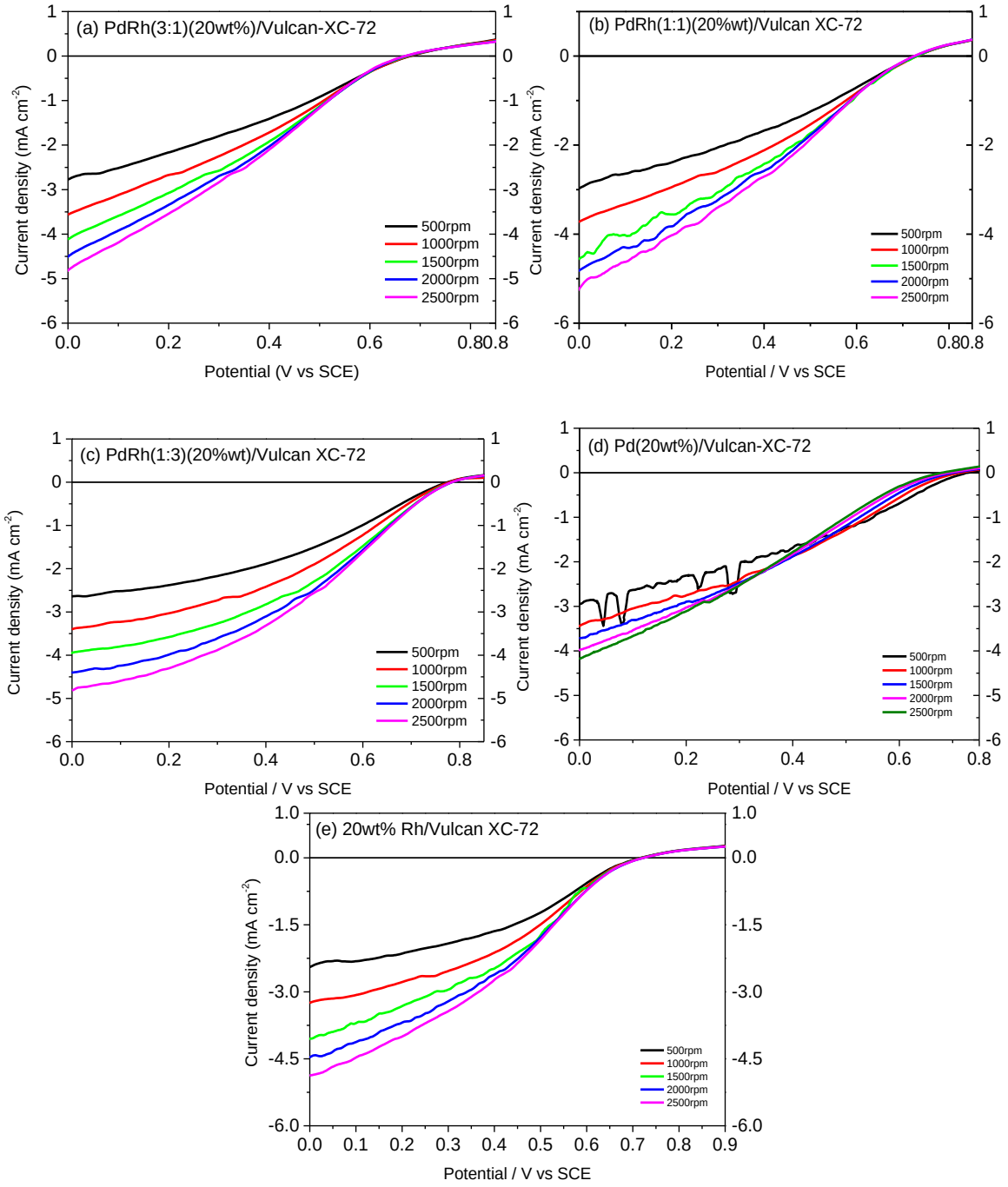

Figure 4.9. RDE curves in H_2-saturated 0.5 M H_2SO_4 at 5 mvs^{-1} for a)PdRh(3:1)/Vulcan XC-72, b) PdRh(1:1)/Vulcan XC-72, c) PdRh(1:3)/Vulcan XC-72, d)Pd/Vulcan XC-72 and e) Rh/Vulcan XC-72.

Moreover in order to calculate the total electrons that take place during ORR we used the Koutecky-Levich equation:

$$i_d = 0.62nFD^{2/3}\nu^{-1/6}C\omega^{1/2}$$

Where n is the number of electrons involved in the reaction, F is the Faraday constant (96485 C/mol), D is the diffusion coefficient of O_2 in the H_2SO_4 (1.4×10^{-5} $cm^2\,s^{-1}$), v is the kinematic viscosity of the electrolyte (1.0×10^{-2} $cm^{-2}\,s^{-1}$), C is the O_2 concentration in the

electrolyte (1.1×10^{-6} mol cm^{-3}). From the slope of the Koutecky-Levich plots the electrons were calculated [60].

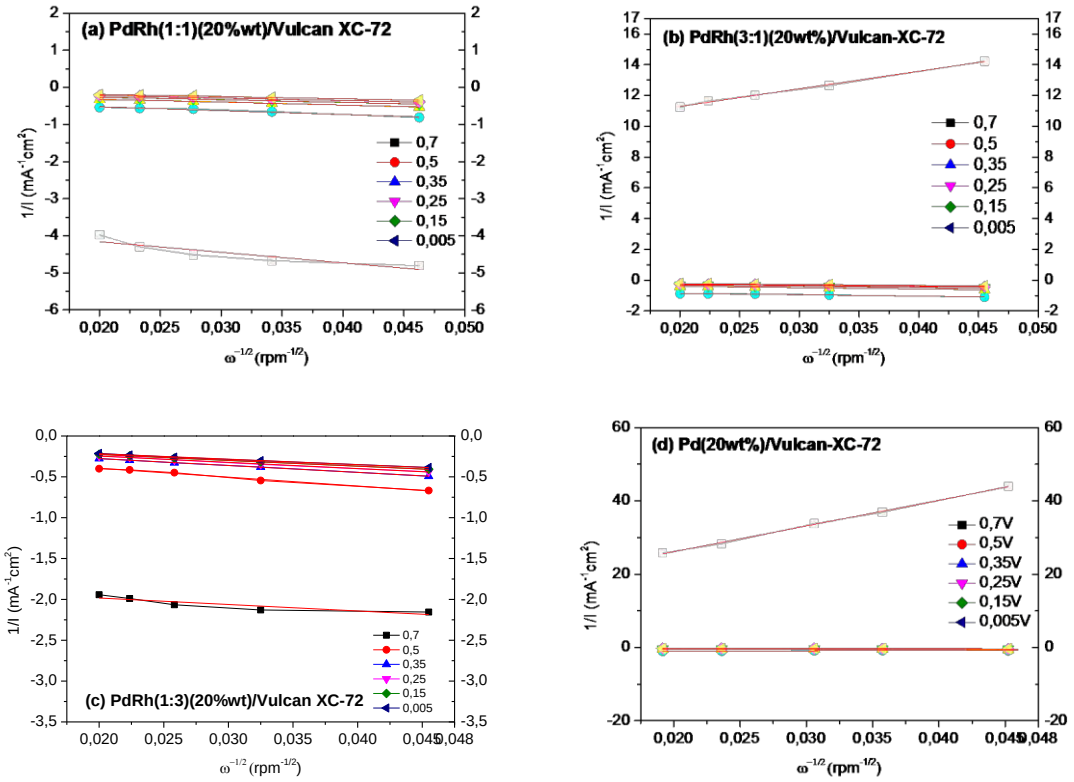

Figure 4.10. Koutecky - Levich plots for the oxygen reduction reaction.

Table 4.3.Kinetic current densities (i_k) for Pd_xRh_x and their ratios in ORR.

Electrode 20%wt (metal loading)	Tafel slope (mV $decade^{-1}$)	I_0 (mA cm^{-2})	i_k (@0.1V) (mA cm^{-2})
Pd/ Vulcan XC-72	131	0.03	0.58
PdRh(3:1)/ Vulcan XC-72	140	0.04	0.89
PdRh(1:1)/Vulcan XC-72	149	0.21	2.10
PdRh(1:3)/Vulcan XC-72	110	0.65	5.20
Rh/ Vulcan XC-72	111	0.1	1.87

The HOR/HER kinetic current densities (i_k) of Pd_xRh_x in oxygen reduction are shown in Fig. 4.11 which was obtained from correcting the polarization curves by the measured iR and the hydrogen mass transport in the HOR branch.

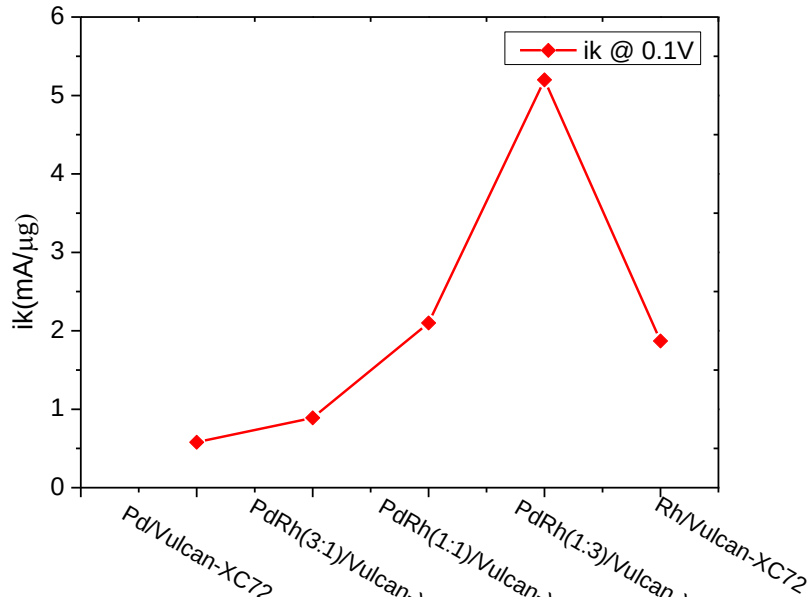

Figure 4.11. i_k for Pd_xRh_x in oxygen reduction.

In order to do further kinetic analysis the mass transfer corrected Tafel equation was adopted:

$$\log(i_k) = \log(i_o) + (\frac{anF}{2.303RT})\eta$$

From Tafel plot (logI vs. η) can be derived the exchange current density (i_0) value that gives relative rates of reaction at equilibrium being calculated from the intercept at y-axis at the region (20 to 50 mV vs. SCE).

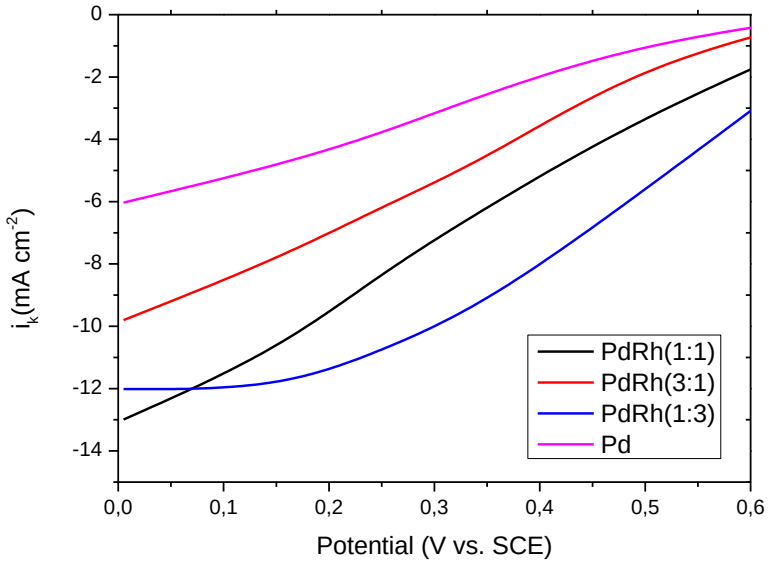

Figure 4.12. Tafel plots for the oxygen reduction reaction.

In Fig 4.12, the calculated exchange current density is compared. It is found to has the following order: 20%PdRh (1:1)> 20%PdRh(1:3) > 20%PdRh(3:1) > 20%Pd, respectively.In all cases Pd loading equals to 11 μgcm^{-2}.The increase of Rh loading seems to affect positively the electrocatalysts' behavior.

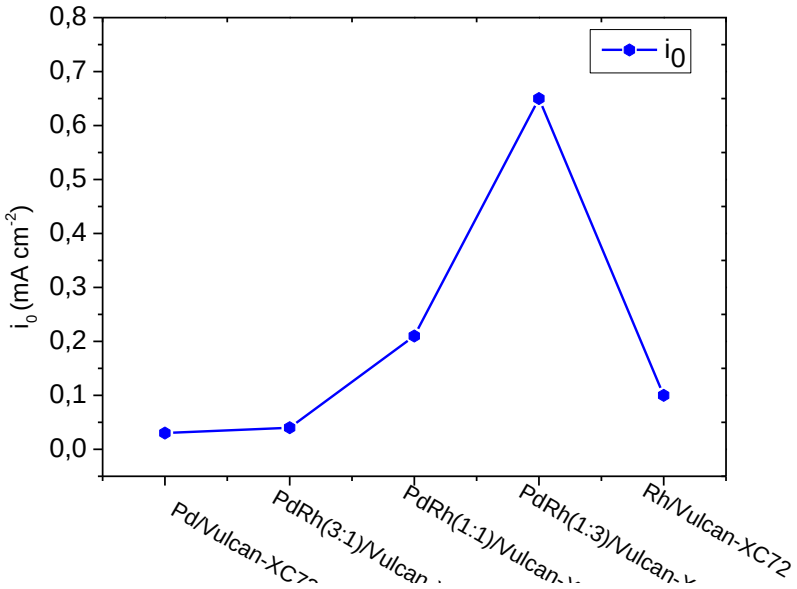

Figure 4.13. i_0 for Pd_xRh_x in oxygen reduction.

In order to have a better understanding about the effect of Rh activity (to the kinetic and exchange current) of the examined electrocatalysts, Fig 4.13 is given. From this it can be derived that pure palladium and high palladium loading (Pd3Rh) do not enhance the oxygen reduction reaction in comparison with the other electrocatalysts (Rh, PdRh and PdRh3) in terms of both exchange current and kinetic density densities. The increased electrocatalytic activity of PdRh bimetallic electrocatalysts could be attributed to their ability to adsorb more hydrogen than Pd [61].

4.2.4. Chronoamperometric measurements

The stability and durability of the examined electrocatalysts Pd_xRh_x for hydrogen electrooxidation in 0.5M H_2SO_4 at 25 °C for 1300s was investigated by chronoamperometric measurements (Fig 4.12) [60].

The rapid development of poisoning species due to the formation of intermediate species (e.g. CHO_{ads} and CO_{ads}) is responsible for the rapid decay of the current densities. As can in Fig. 5.3. PdRh(1:3)/Vulcan XC-72 catalyst appears to have the same current

decay with PdRh(1:1)/Vulcan XC-72 after 200s, however, after 200s PdRh(1:3)/Vulcan XC-72 show better long term stability.

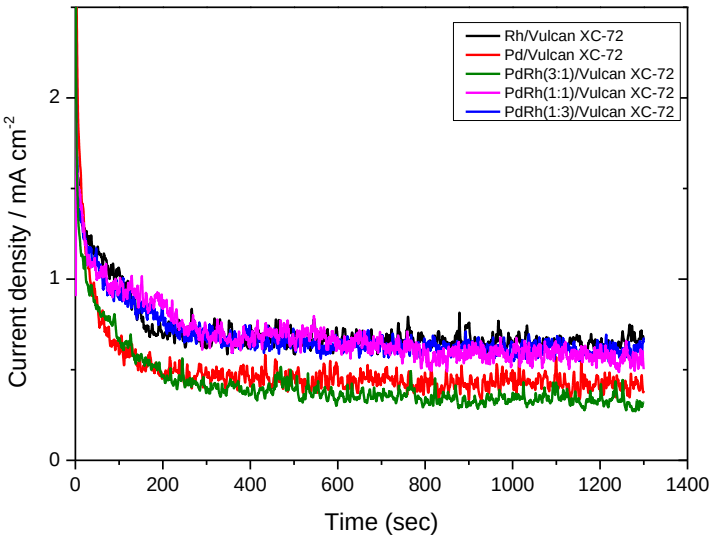

Figure 4.14. Chronoamperometry curves for hydrogen oxidation in 0.5M H_2SO_4 for 1300 sec at -0.25V.

CHAPTER 5

5. CHARACTERIZATION OF PdxPty BASED ANODES AND CATHODES FOR HYDROGEN OXIDATION AND OXYGEN REDUCTION REACTIONS

In Chapter5 carbon Vulcan XC-72R supported PdxPtx (x=99:1, 98:2, 97:3) nanoparticles have been prepared by a modified pulse microwave assisted polyol method and have been studied for hydrogen electrooxidation in sulphuric acid media. The PdxPtx/C electrocatalysts have been characterized by X-ray diffraction (XRD), Transmission Electron Microscopy (TEM), Cyclic Voltammetry (CV), Rotating Disk Electrode (RDE) and Chronoamperometric measurements (CA).

The effects of the concentration of electrolyte and PdxPtx as well as of temperature on the activity of hydrogen electrooxidation have been investigated. According to the results, the electro-catalytic activity towards hydrogen electrooxidation of the investigated catalysts has the following order: PdPt (98:2)/C>PdPt (97:3)/C>PdPt (99:1)/C>Pd/C.

5.1 Physicochemical measurements of Pd_xPt_x

XRD patterns of the as-prepared electrocatalysts are shown in Fig 5.1. The first peak at 25° is associated with the Vulcan XC-72 support material for all the five samples.

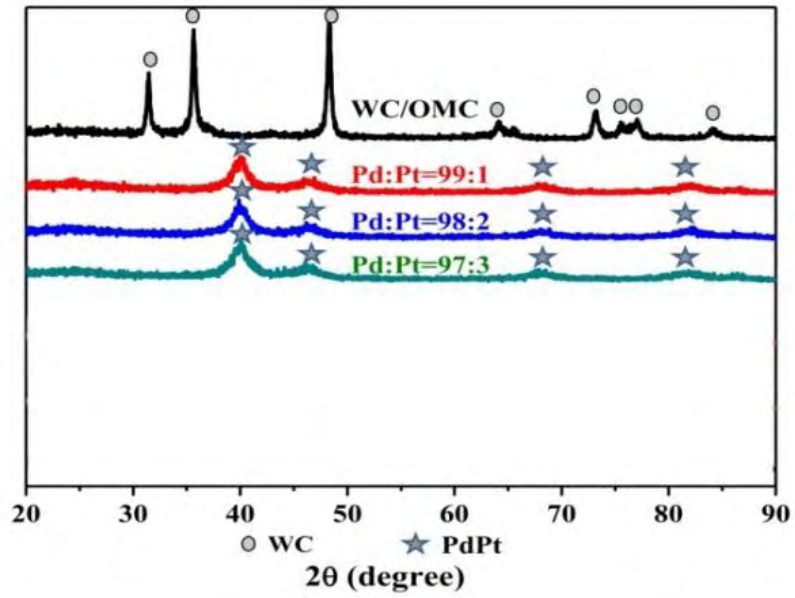

Figure 5.1. XRD patterns of WC/OMC and Pd_xPt_y/C.

The diffraction peaks of Pd_xPt_y/C catalysts are at about 40◦, 46◦, 68◦ and 81◦ and attributed to the (1 1 1), (2 0 0), (2 2 0) and (3 1 1) planes of the face center cubic (FCC) structure of the Pd–Pt alloys. The mass ratio of Pd/Pt has a slight effect on the crystalline structure due to similar crystalline structures of Pt and Pd [62].

In order to examine the surface morphology of the prepared electrocatalysts with PdPt and their ratios, TEM images are shown in Fig. 5.2.

From the pictures listed below we can draw the conclusion which catalyst has the best dispersion on the surface of the prepared electrocatalysts. Better dispersion has PdPt (99:1), as we can see from Fig. 5.2. (c) then follows PdPt(98:2) (b) and PdPt(97:3) (a). In the figure above is shown that the dispersion that was made in PdPt(97:3) was not very correct and is not all across the surface area that we are interested and examine [62].

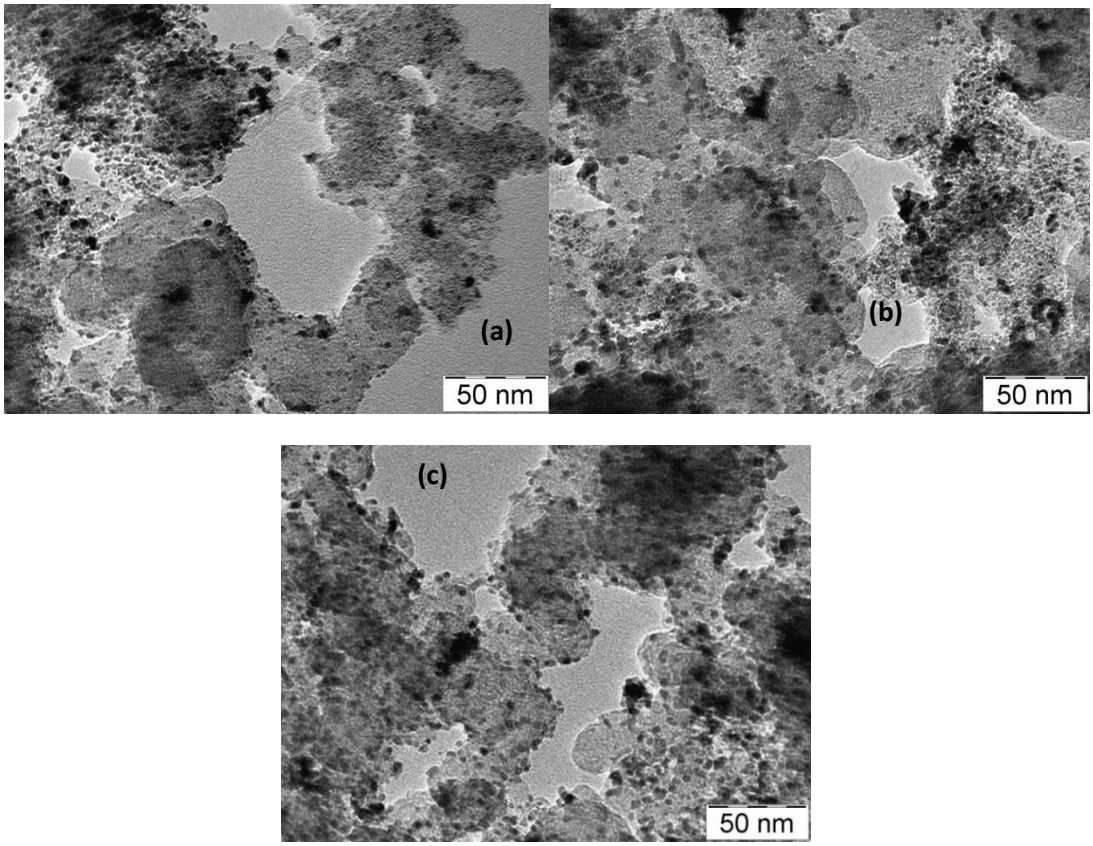

Figure 5.2. TEM images of (a) PdPt(97:3)(20%)/Vulcan XC-72, (b) PdPt(98:2) (20%)/Vulcan XC-72, (c) PdPt(99:1) (20%)/Vulcan XC-72.

5.2 Electrochemical active surface area- Cyclic voltammetry measurements

As in the Pd_xRh_x electrocatalysts, in this sample we use the same method, cyclic voltammetry. The conditions remain the same, in order for us to have a yardstick, so we are expecting a characteristic voltammogram and its electrochemical output to be different than the tested catalysts with rhodium. The surface of noble metal alloy can be characterized by identifying the distinctive CV features associated with each component.

Fig.5.3 shows the voltammetric profiles of the as-prepared bimetallic films obtained in 0.5 M H_2SO_4 solution at the scan rate of 50 mV s^{-1}. CV was performed to determine the electrochemical surface area and to elucidate the adsorption properties of the catalyst.

For a positive-going sweep the first peak (at 0 to ~0.15V versus SCE) represents hydrogen desorption region. The oxidation/reduction peaks corresponding to the formation of iridium oxide during the cathodic scan may be observed in at around 0,6 V (SCE). The redox peaks in the 0.8–1.2 V region corresponding to the formation and reduction of surface Pd oxides (Pd–OH or PdOx species). It is known that the PdOx species at the metallic Pd surface is inactive toward oxygen reduction [62].

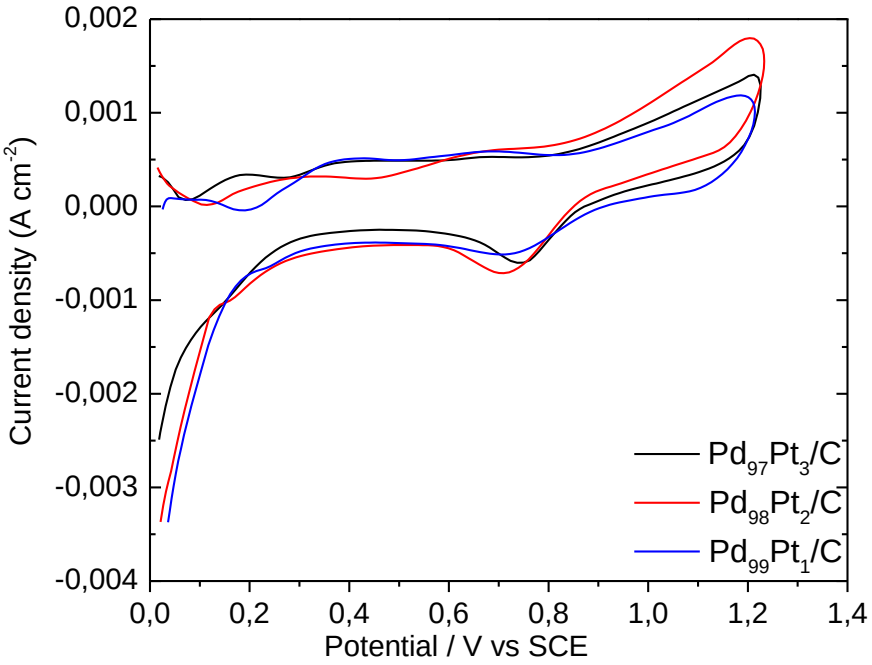

Figure 5.3. Cyclic voltammograms for PdPt(97:3)(20%wt)/Vulcan XC-72,PdPt(98:2)(20%wt)/ Vulcan XC-72 and PdPt(99:1)(20%wt)/Vulcan XC-72 in 0.5 M H2SO4 de-oxygenated and saturated with He, the potential scan speed is 50 mV s^{-1}.

In order to evaluate the electrochemical active surface area of the as prepared electrocatalysts cyclic voltammetry measurements were conducted in 0.5 M H_2SO_4 (Figure 5.3), for 50 mV s^{-1}. In the case of Pd-based electrocatalysts the electrochemical active surface area (ECSA) is calculated by determining the coulombic charge (Q) for the reduction of palladium oxide peak.

$$ECSA\left[\frac{m^2}{g}\right] = \frac{Q_H}{Q_{(Pd)} \times m_{Pd} \times 10}$$

Where Q_H represents the charge of the reduction peak, Q_{Pd} =420μC cm_{Pd}^{-2} are the specific amount of electricity corresponding to the full coverage of the Pd surface by one monolayer of oxygen (μCcm^{-2}) and m_{Pd} ($mg\,cm_{electrode}^{-2}$) is the palladium loading on the working electrode's surface.

The electrochemical active surface areas have the following order: Pd97Pt3/C (17.0 m^2 g^{-1}) > Pd98Pt2/C (5.2 m^2 g^{-1}) > Pd99Pt1/C (3.5 m^2 g^{-1}). Increasing platinum's content the electrochemical active surface area is increasing.

Table 5.1.Electrocatalytic kinetic parameters on different electrodes in 0.5 mol L^{-1} H_2SO_4, at 25 °C, 50 mV s^{-1}.

Electrode 20%wt	Pd loading ($\mu g\ cm^{-2}$)	Q_H ($mC\ cm^{-2}$)	ECSA $(m^2\ g^{-1})_{Pd}$
PdPt(99:1)/Vulcan XC-72	10.8	0.32	1.95
PdPt(98:2)/Vulcan XC-72	10.6	0.46	2.50
PdPt(97:3)/Vulcan XC-72	10.4	1.6	2.20

5.3. Hydrogen oxidation reaction measurements

The presented results show that the prepared electrocatalysts have a high loading for the hydrogen oxidation reaction. Figure 5.4 shows the HOR polarization curves on Pd_xPt_x in 0.5M H_2SO_4 at room temperature as a function of rotation rate, with well-defined hydrogen mass transport controlled current densities occurring at potentials above0.05V.

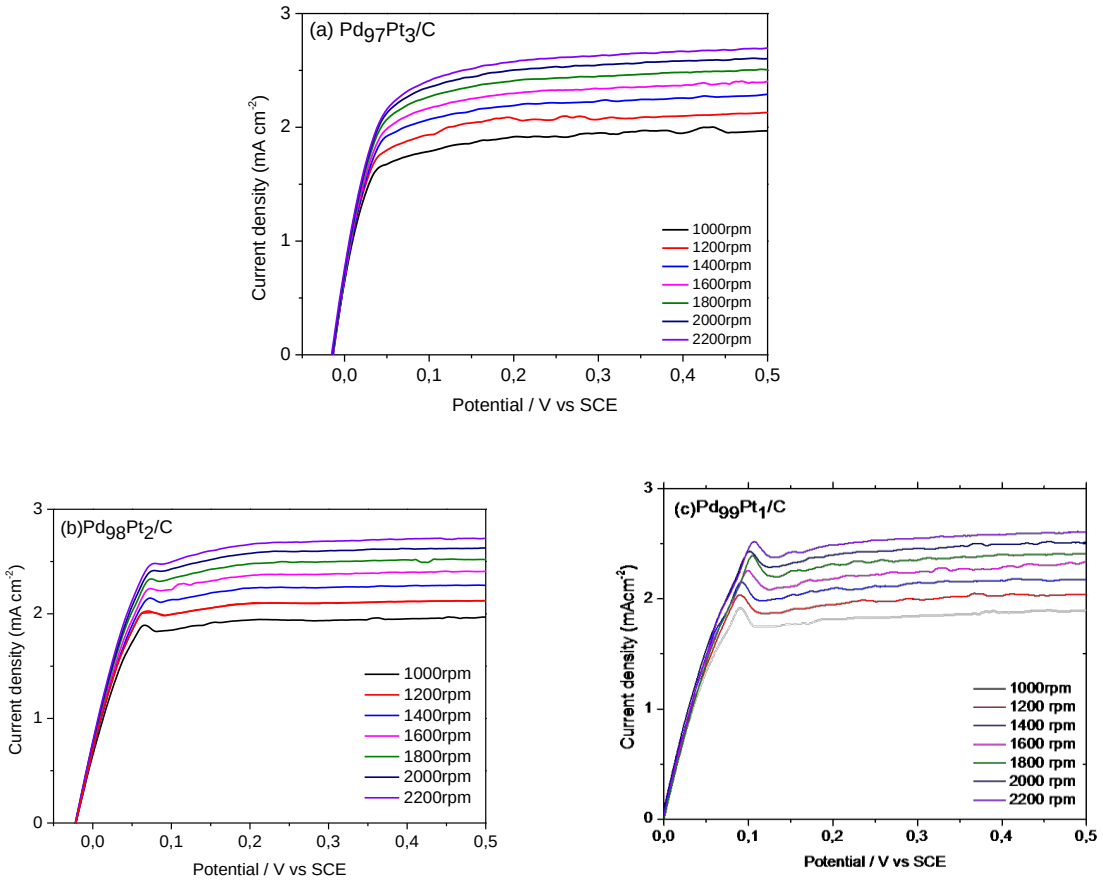

Figure 5.4RDE curves in H_2-saturated 0.5 M H_2SO_4 at 5 mvs^{-1} for a)PdPt(97:3)/Vulcan XC-72, b)PdPt(98:2)/Vulcan XC-72, c)PdPt (99:1)/Vulcan XC-72.

In order to determine the catalytic activity of the material, we analyzed the Koutecky–Levich analysis, where the catalytic current is related to the rotation rate of the RDE. It is

generally accepted that the hydrogen electrode reaction on a metallic surface is verified through the elementary steps of Tafel, Heyrovsky, and Volmer as mentioned in the HOR measurements of PdxRhy.

Table 5.2.Kinetic current densities (i_k) for Pd_xPt_x in HOR.

Kinetic current density (mA/cm^2)				
Catalysts	Pd/C	PdPt(97:3)	PdPt(98:2)	PdPt(99:1)
Potential (V)				
0,015	0,39193	5,6243	2,20429	1,55321
0,05	**1,17965**	**4,56863**	**7,11797**	**2,46749**
0,15	3,60257	9,11797	12,19754	9,8668
0,5	4,7619	11,57273	13,6668	12,09629

The measured total current density in RDE was composed of the kinetic current density (j_k) and diffusion limited current density (j_d) since the film resistance of Nafion is sufficiently small. Therefore, Koutecky–Levich equation is following as:

$$\frac{1}{i} = \frac{1}{i_k} + \frac{1}{i_d}$$

Where i is the experimental value of the current, i_k represents the kinetic current in the absence of mass transfer limitations and i_d is the diffusion-limited current. The later can be calculated according to the Levich equation:

$$i_d = 0.62nFD^{2/3}\nu^{-1/6}C\omega^{1/2}$$

Where n is the number of theoretically-transferred electrons (=2), F the Faraday constant (96485 C/mol), D the diffusion coefficient of H_2 in the H_2SO_4, v the kinematic viscosity of the electrolyte and C the H_2 concentration in the electrolyte of the dissolved-oxygen at an oxygen partial pressure of 1 bar ($1.26\ 10^{-6}$ mole cm^{-3});. The kinetic current density was graphically determined ($1/i$ vs. $1/\omega^{1/2}$ - Koutecky-Levich plots).

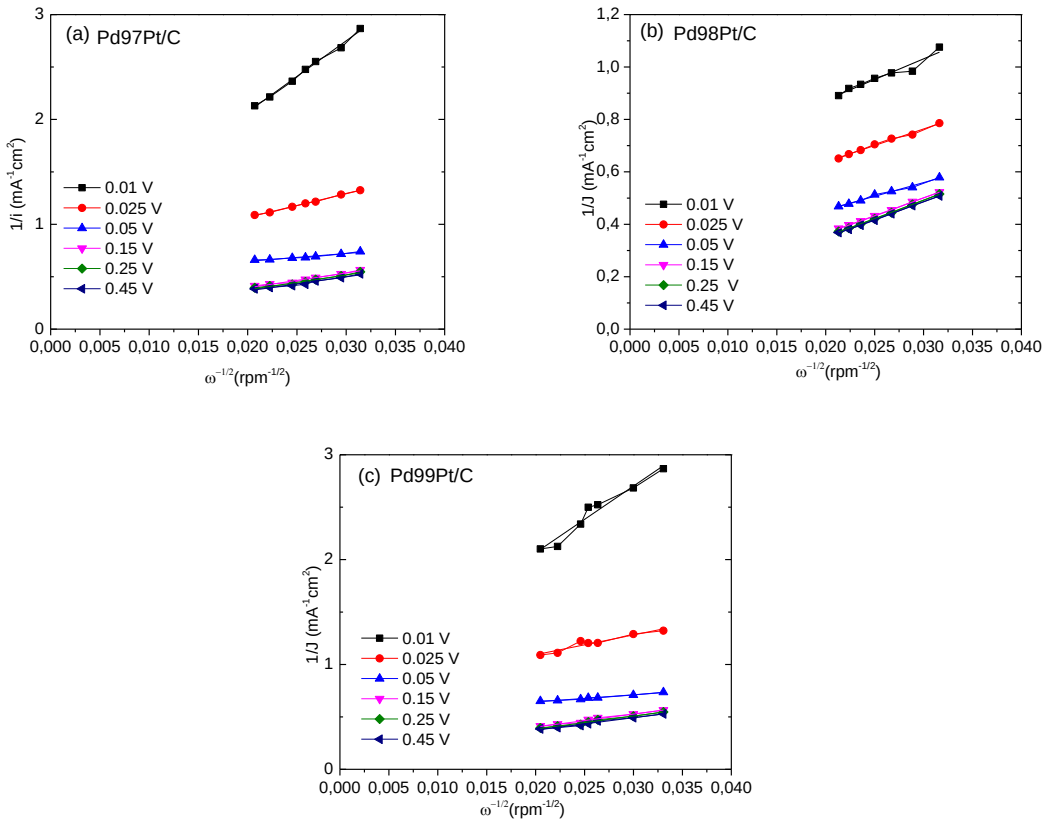

Figure 5.5. Koutecky – Levich plots for the hydrogen oxidation reaction.

The HOR kinetic current densities (i_k) on Pd_xPt_x are shown as green bars in Fig. 5.6which were obtained from correcting the polarization curves by the measured iR and the hydrogen mass transport in the HOR branch.

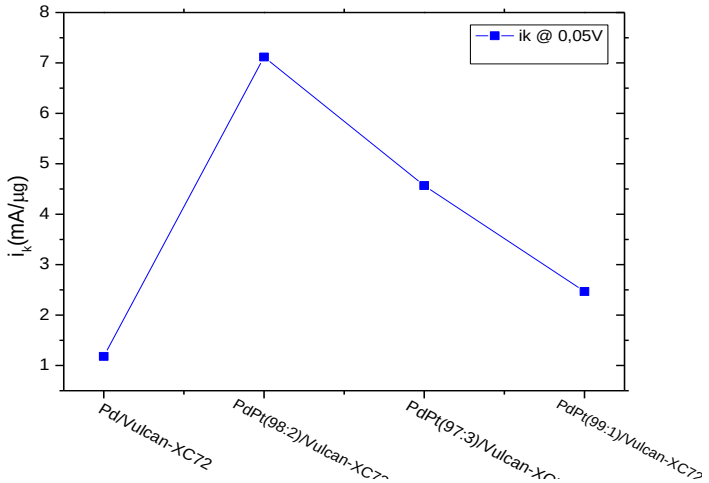

Figure 5.6. i_k for Pd_xPt_x in hydrogen reduction.

In order to do further kinetic analysis the mass transfer corrected Tafel equation was adopted:

$$\log(i_k) = \log(i_o) + (\frac{anF}{2.303RT})\eta$$

From Tafel plot (logI vs. η) can be derived the exchange current density (i_0) value that gives relative rates of reaction at equilibrium being calculated from the intercept at y-axis at the region (20 to 50 mV vs. SCE).

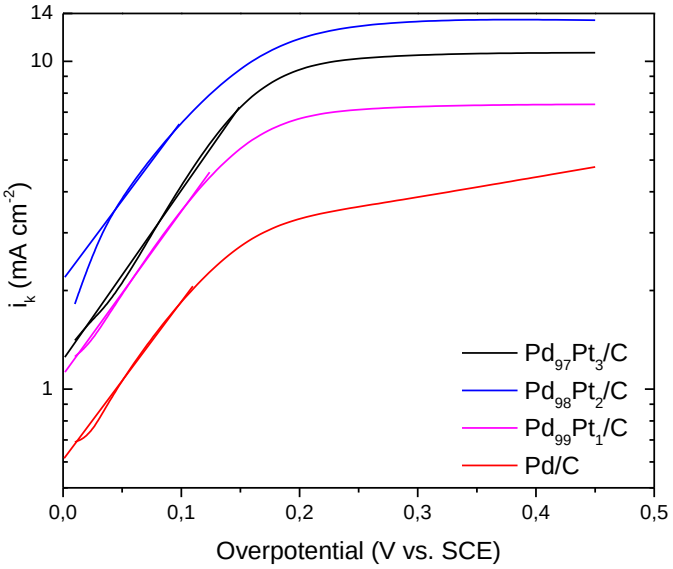

Figure 5.7. Tafel plots for the hydrogen reduction reaction.

From Fig 5.7, the exchange current density was calculated 7.11,4.56, 2.46 and1.17mA cm^{-2} following the order: Pd98Pt2/Vulcan XC-72>Pd97Pt3/Vulcan XC-72 >Pd99Pt1/Vulcan XC-72 >Pd/Vulcan XC-72 in each electrolyte. In all cases Pd loading equals to 11 μgcm^{-2}.The increase of platinum loading seems to affect positively the electrocatalysts' behavior.

5.4. Oxygen reduction reaction measurements

Figure 5.8 shows the ORR polarization curves on Pd_xPt_x in 0.5M H_2SO_4 at room temperature as a function of rotation rate, with well-defined hydrogen mass transport controlled current densities occurring at potentials above 0.05V.

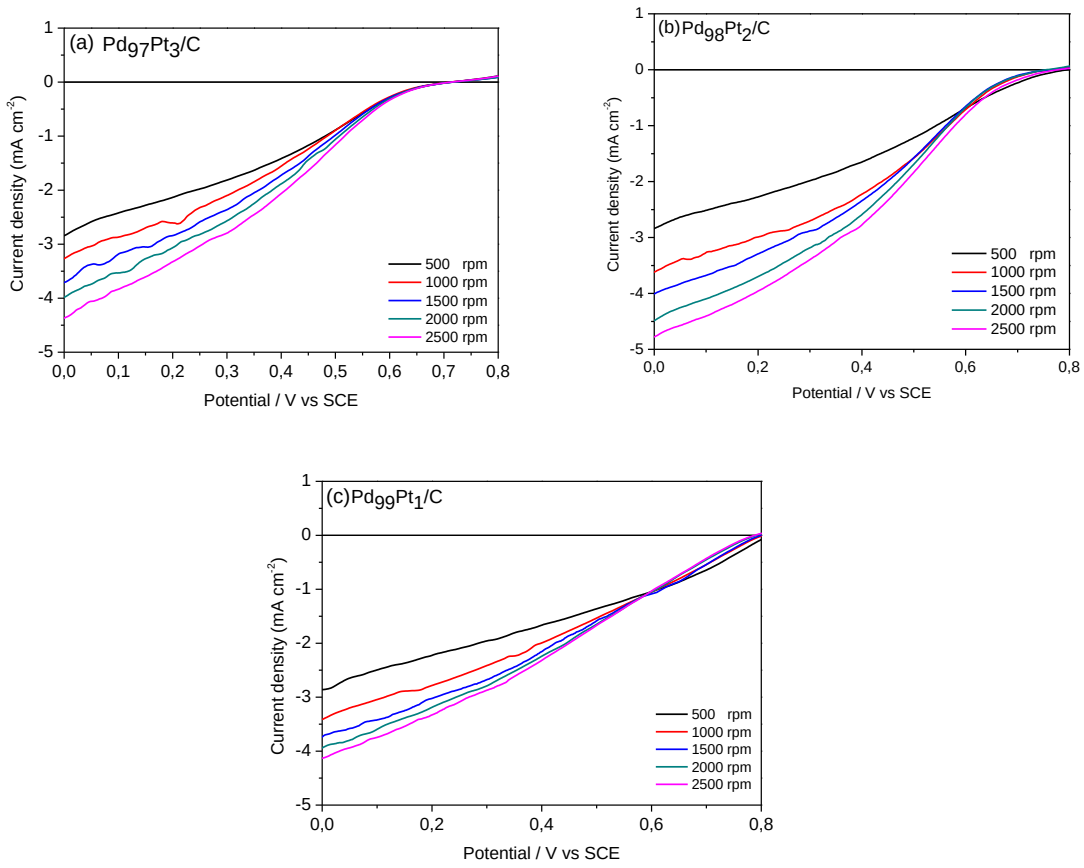

Figure 5.8. RDE curves in H_2-saturated 0.5 M H_2SO_4 at 5 mvs^{-1} for a)PdPt(97:3)/Vulcan XC-72, b) PdPt(98:2)/Vulcan XC-72, c) PdPt(99:1)/Vulcan XC-72. The insets are the corresponding to the Koutecky-Levich plots for the oxygen reduction reaction.

We can observe from ORR curves in Fig.5.8 that while adding Pt to a Pd catalyst, this results in improving the catalyst's ORR activity in certain ratios. With PdPt(98:2) giving the highest current density, the ratio PdPt(97:3) follows and then the current density is lower in the ratios PdPt(99:1).

Moreover in order to calculate the total electrons that take place during ORR we used the Koutecky-Levich equation:

$$i_d = 0.62nFD^{2/3}\nu^{-1/6}C\omega^{1/2}$$

Where n is the number of electrons involved in the reaction, F is the Faraday constant (96485 C/mol), D is the diffusion coefficient of O_2 in the H_2SO_4 (1.4×10^{-5} $cm^2\,s^{-1}$), v is the kinematic viscosity of the electrolyte (1.0×10^{-2} $cm^{-2}\,s^{-1}$), C is the O_2 concentration in the electrolyte (1.1×10^{-6} mol cm^{-3}).From the slope of the Koutecky-Levich plots the electrons were calculated.

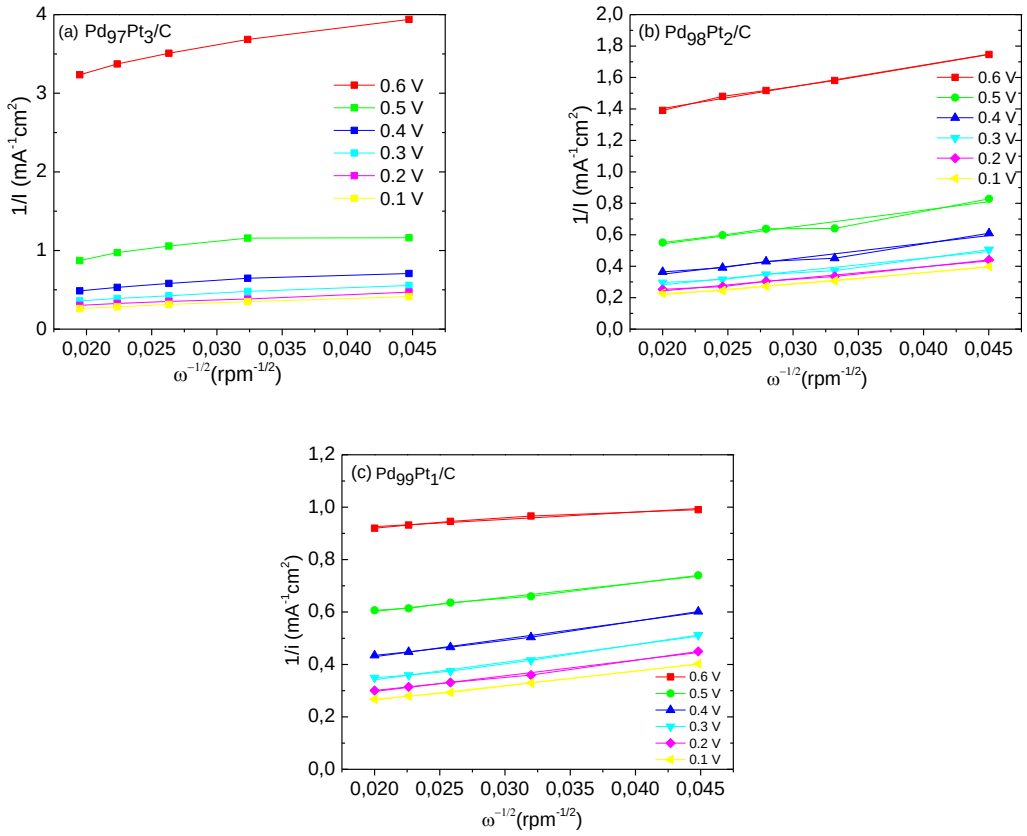

Figure 5.9. Koutecky – Levich plots for the oxygen reduction reaction.

This is a contradicting fact with the catalysts with PdPt and their ratios, because it was expected that while adding platinum in the palladium catalysts, which would result in better kinetic current densities.

Table 5.3. Kinetic current densities (i_k) for Pd_xRh_x and their ratios in ORR.

	Kinetic current density (mA/cm^2)			
Catalysts / **Potential (V)**	Pd/C	PdPt(97:3)	PdPt(98:2)	PdPt(99:1)
0.7	0,07932	-0,27858	-0,54808	0,11092
0.5	**-0,88632**	**-3,21099**	**-5,6319**	**-1,5015**
0.35	-2,51294	-6,16333	-9,26612	-4,62599
0.25	-3,81577	-8,28981	-10,79447	-6,16751
0.15	-4,84896	-10,80847	-12,02212	-7,85608
0.005	-6,03209	-12,99545	-12,01634	-9,80296

The HOR kinetic current densities (i_k) of Pd_xRh_x in oxygen reduction are shown as blue line in Fig. 5.10 which were obtained from correcting the polarization curves by the measured iR and the hydrogen mass transport in the HOR branch.

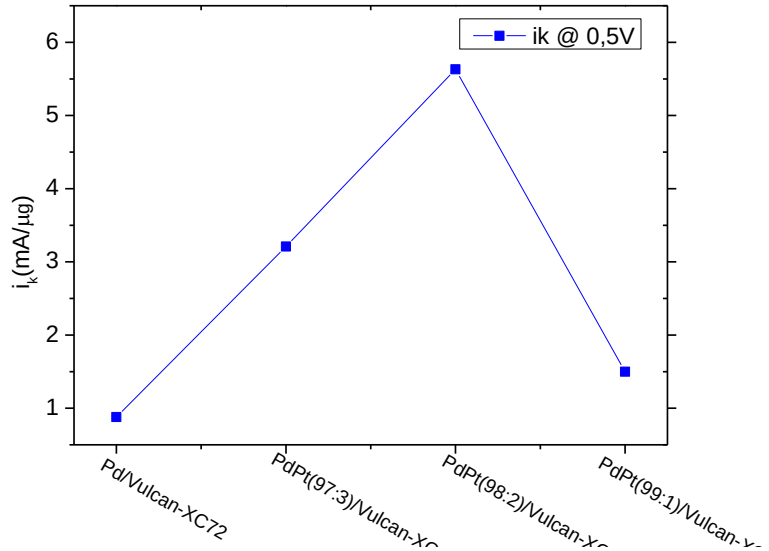

Figure 5.10. i_k for Pd_xRh_x in oxygen reduction.

In order to do further kinetic analysis the mass transfer corrected Tafel equation was adopted:

$$\log(i_k) = \log(i_o) + (\frac{anF}{2.303RT})\eta$$

From Tafel plot (logI vs. η) can be derived the exchange current density (i_0) value that gives relative rates of reaction at equilibrium being calculated from the intercept at y-axis at the region (20 to 50 mV vs. SCE).

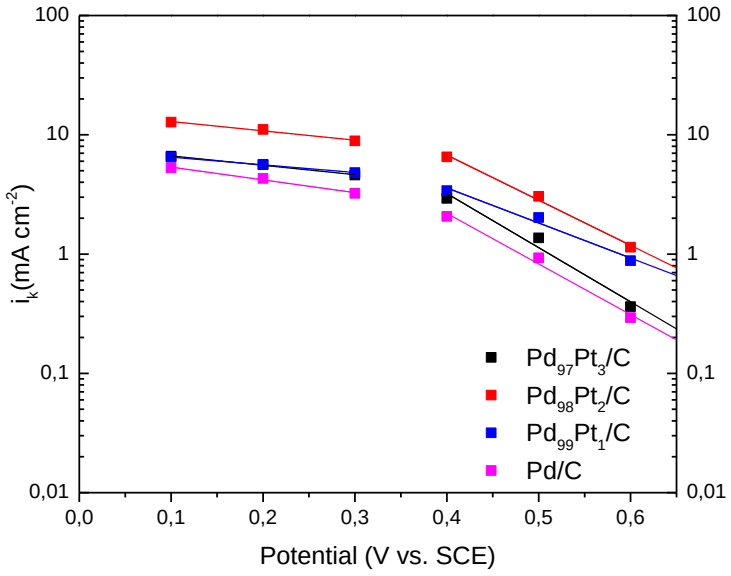

Figure 5.11. Tafel plots for the oxygen reduction reaction.

5.5. Chronoamperometric measurements

The stability and durability of the examined electrocatalysts Pd_xPt_x for hydrogen electrooxidation in 0.5M H_2SO_4 at 25 °C for 1300s was investigated by chronoamperometric measurements (Fig5.12).

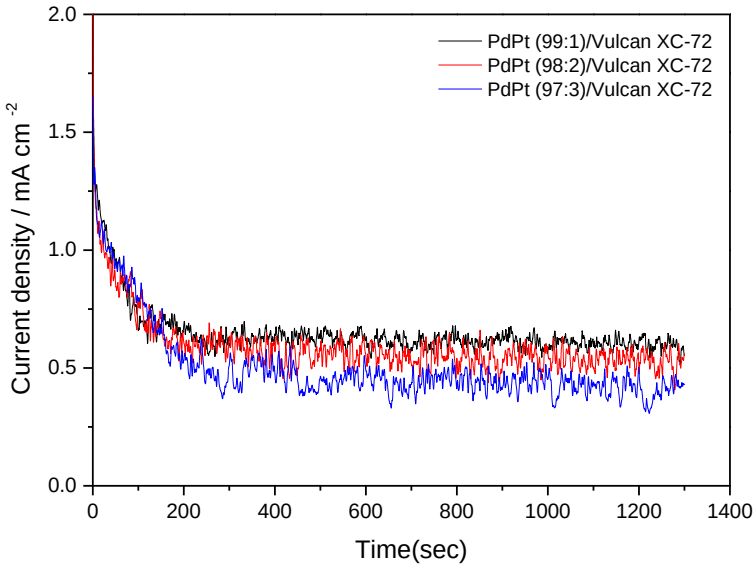

Figure 5.12. Chronoamperometry curves for hydrogen oxidation in 0.5M H_2SO_4 for 1300 sec at -0.25V.

The rapid development of poisoning species due to the formation of intermediate species is responsible for the rapid decay of the current densities. As can in Fig. 5.8 PdPt(99:1)/Vulcan XC-72 catalyst appears to have the same current decay with PdPt(98:2)/Vulcan XC-72 after 200s, however, after 200s PdPt(99:1)/Vulcan XC-72 show better long term stability.

CHAPTER 6

6. PEM FUEL CELL RESULTS & ANALYSIS

In Chapter 6, an electrochemical characterization of the homemade fuel cell MEA is made. The used membrane is $Pd_{97}Pt_3$/C. The preparation of the fuel cell is analyzed and the tests made in order to check the anode and the cathode of the fuel cell for leakages.

The measurements before the catalytic activation of the MEA ae presented and the chapter concludes with the presentation of the distinctive polarization curves of the fuel cell regarding measurements in different temperatures.

As the temperature rises, we are able to observe losses in the fuel cell. Further investigation is due to experimentation at the moment.

6.1. Electrochemical characterization

In this thesis, we are analyzing a homemade membrane $Pd_{97}Pt_3$/C. Initially we tested for comparison a membrane with Pt (60wt%) / C / / Nafion212 / / Pt (60wt%) / C (Fuel Cells ETC), with 0.5mgPtcm^{-2} at the anode and 0.5mgPtcm^{-2} at the cathode. The thicknesses of both films are up to 410mm.

6.1.1. Preparation of the fuel cell

The membrane is placed into the bipolar plates by applyingtorque9Nm.Beforestartingthe measurements, the fuel cell is checked for leaks of the fuel from the anode to the cathode and vice versa. The control of leakage (diffusion fuel oxidant / cathode) is the measure of securing the insulation film. For absolute control an inert gas should be used, preferably helium, which represents the leakage of hydrogen. Nitrogen and argon are preferably to be inserted second so as to be used.

The gas bottle is connected (without flow meters) in the fuel inlet of the fuel cell. The output of the fuel (anode) is blocked. At the outlet of the oxidizing agent bubble flowmeter is connected.

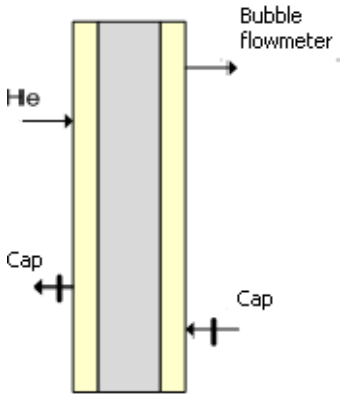

Figure 6.1. Schematic connections for leak testing of the fuel (anode) to the oxidant (cathode).

On the anode side the pressure is slowly increased (1.5 bar maximum) allowing the system to equilibrate. The balance of the system varies from a few seconds to a few minutes, depending on the size of the fuel cell and the shape of flow channels. The experimental apparatus used for the present measurements requires a few seconds. The output of the anode is blocked and with a bubble flowmeter it is controlled whether there is flow at the outlet of the cathode. If there is no leakage from the anode to the cathode through the membrane, there will be no flow to the flowmeter and bubble.

We also have to check for leakage of the oxidant gas to the fuel. The leak test of oxidant to fuel (cathode to anode) aim is to ensure further the completeness of the film. During the inspection of leaks, the gas bottle (without flowmeters) is connected to the input of the oxidant (cathode) of the fuel cell. The output of the oxidant (cathode) is blocked by the cap. At the output of the fuel (anode) bubble flowmeter is connected.

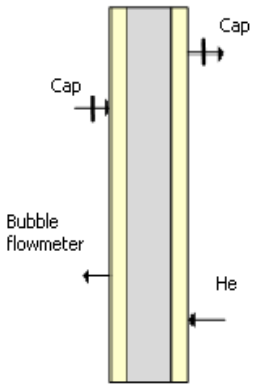

Figure 6.2. Schematic connections for leak testing from the oxidant (cathode) to the fuel (anode).

The pressure of the cathode side is slowly increased (1.5 bar maximum) and we allow the system to equilibrate. As mentioned above, the time needed to balance the system ranges a few seconds.

The output of the cathode is plugged while the bubble flow meter monitors whether there is flow at the outlet of the anode. If there is no leakage from the cathode to the anode there will be no flow to and from the bubble flow meter.

6.2. Measurements before catalytic activation

Initially, by the method of cyclic voltammetry, measurements occurred in order to assess the electrochemical active surface prior to activation of the catalyst layers of the membrane. The experimental conditions were as follows: $T_{in,\,H2} = T_{in,\,He} = 70^{o}C$, $T_{cell} = 70^{o}C$, $T_{sat} = 70^{o}C$, scan rate: 50 mv s^{-1}, RH = 100%.

The dynamic range of the measurements was from 0.001 to1V, as shown in Figure6.3. Measurements were continued up to obtain a stable cyclic voltammogram (5 cycles).

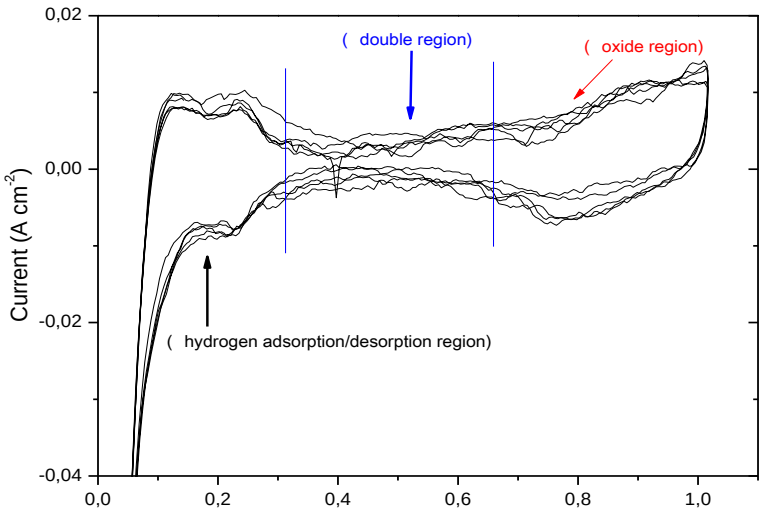

Figure 6.3.Cyclic voltammetry measurements before and after activation T_{cell}=70°C, $T_{in,H2}$=$Ti_{n,He}$=70°C, F_{H2}= 20cc, F_{He}=100cc, scan rate: 50 mv s^{-1}.

From 0.001 to 0.35 V the classical adsorption /desorption curve of hydrogen is displayed. From0.33 to 0.7 V, the slight curve in the bilayer (double layer region) shows the small contribution of carbon to the active surface of the catalyst. Going to more positive potentials as light curve is observed, due to oxide formation. Considering the area of adsorption/ desorption of hydrogen and the following equation, the electrochemical active surface is calculated and the specific surface area of platinum per electrode surface prior to activation, in accordance with equations(1) &(2),

$$ECA(\text{Electrochemical Active Area}) = \frac{Qads + Qdes}{\mu_{Pt} \times L} \quad (1)$$

Where $Q_{\text{before aquation}}=0.020\ \text{C cm}^{-2}_{Pt}$

$$\mu_{Pt}= 0.21*10^{-3}\text{C cm}^{-2}_{Pt})$$

$$L = 1mg_{Pt}\ \text{cm}^{-2}_{geo})$$

$$ASR(Specific\ Area\ of\ \ Platinum) = ECA \times loading(cm^2_{Pt}\ \text{cm}^{-2}_{electrode}) \quad (2)$$

The electrochemical active area is calculated at **ECA**=98514 $cm^2 g_{Pt}^{-1}$ and the specific area of platinum is at **ASR**=98.5 $cm^2_{Pt}\ \text{cm}^{-2}_{electrode}$. In Figure 6.4 a comparative measurements is shown before and after the activation in which the classical absorption/ desorption curve is shown after the 1st and after 500 cycles with the cyclic voltammetry measurements.

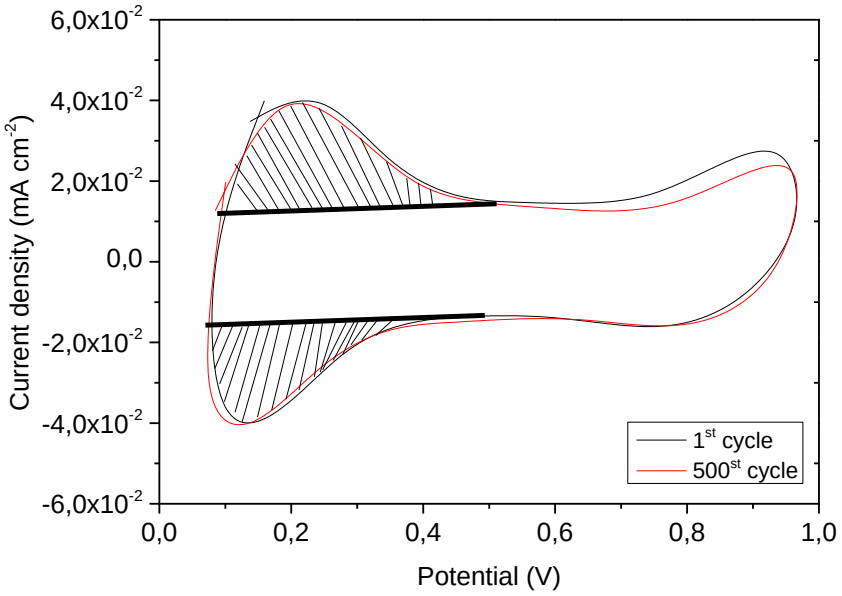

Figure 6.4. Cyclic voltammetry measurements with the absorption/desorption curve is displayed.

6.3. Distinctive polarization curves of the PEM fuel cell

Figure 6.5 gives the typical polarization curve of the fuel cell before activation expressed in terms of power. The temperature of the fuel cell was 80 ° C, while the feed lines and saturate the reactive gas was 90 ° C. The hydrogen flow rate was at 80cc, while oxygen in 40cc. The maximum power recorded is 83 mW cm^{-2} (or 0.083 mW mg_{Pt}^{-1}).

Due to losses resulting from undesired species crossover from one electrode through the electrolyte and the internal currents, the actual open circuit voltage is below the theoretical value. Besides this, there are three major classifications of losses that result in a drop from the open circuit voltage and these are the activation polarization, the ohmic polarization and the concentration polarization.

As you increase the temperature the rate of reaction increases. As a rough approximation, for many reactions happening at around room temperature, the rate of reaction doubles for every 10°C rise in temperature.

Some reactions are virtually instantaneous - for example, a precipitation reaction involving the coming together of ions in solution to make an insoluble solid, or the reaction between hydrogen ions from an acid and hydroxide ions from an alkali in solution. So heating one of these won't make any noticeable difference to the rate of the reaction.

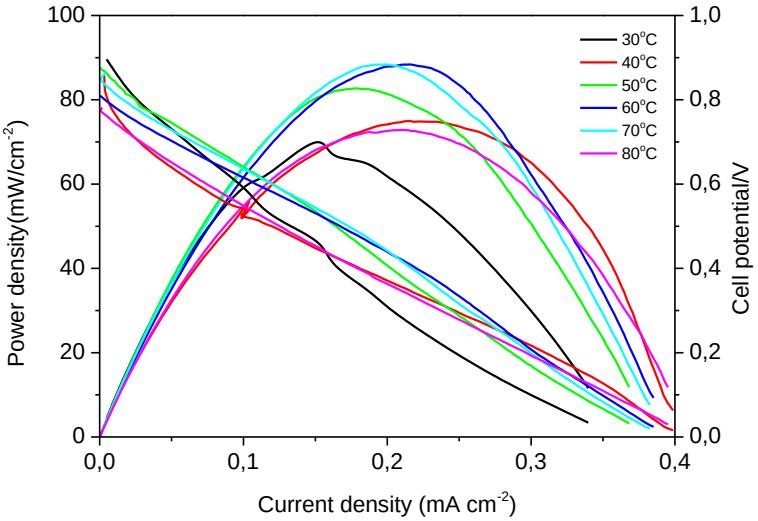

Figure 6.5. Operating curves of the PEM fuel cell in various temperatures.

Activation and concentration polarization occurs at both anode and cathode locations, while the resistive polarization represents ohmic losses throughout the fuel cell. Activation polarization, which dominates losses at the low current densities, is the voltage overpotential required to overcome the activation energy of the electrochemical reaction on the catalytic surface, and is thus heuristically similar to the activation energy of purely chemical reactions.

CHAPTER 7

7. CONCLUSIONS AND PERSPECTIVES

This very last part summarizes the scientific results of research done in the framework of the present MSc dissertation. At the same time some outlooks for further continuation of this research are provided. Hydrogen electrooxidation and especially oxygen reduction have been the research topic due to the importance of great growth of the PEM technology in the modern world. General, whatever the fuel that is used in a fuel cell, Pt considers the first and most widely investigated material for fuel (hydrogen, methanol, ethanol, methane) electrooxidation in sulphuric acid media. For hydrogen electrooxidation Pt is a very suitable catalyst due to its high efficiency and its poor selectivity of different substances presented during the electrooxidation reactions. Preparation method is a very important parameter for catalysts' preparation as it affects their properties (lattice parameter, diameter of nanoparticles, catalysts dispersion on the support). A modified pulse - microwave assisted polyol method was chosen because of the following remarkable advantages: i) rapid volumetric heating, ii) higher reaction rate and selectivity, iii) shorter reaction time and iv) higher yield of the product compared to the convention heating methods. Therefore, the use of microwave heating is more popular in scientific world.

In the first part of the dissertation a general introduction gave all the necessary information in order to cope with the electrochemical nature of fuel cells. A classification of fuel cells and the structure of every form were mentioned.

Specifically, the dissertation focused on the proton exchange membrane fuel cells and their anatomy (gas diffusion layers, bipolar plates and membranes) with an analytical study.

The advantages and disadvantages of fuel cells were noted and how their use could affect peoples' everyday life.

Then, a thermodynamic analysis is noted with all the necessary information included.

In the experimental part, the conclusions that are made are that:

1. While studying the electrochemical and the physicochemical measurements of Pd_xRh_x, the conclusion that is made is that the ECSA is higher when the ratio is 1:1.
2. Furthermore, in the study of Pd_xPt_x the conclusion that is made is that the stability of the catalysts is not very accurate and further measurements need to be taken – with both homemade and commercial catalysts- in order to assure stability and logical results.
3. According to the experimental results and the kinetic analysis, the addition of a little amount of platinum to pure palladium electrocatalyst enhances electrocatalytic activity towards HOR and ORR.
4. Further studies are enhanced in the direction of the palladium catalysts and the use of platinum in anode and cathode processes.
5. Regarding now the measurements taken in the PEM fuel cell, the experimental results were coherent with the bibliography and further study is being done at the moment with MEAs' with different amount of platinum.
6. The MEA that it was studied in the laboratory, gave the results that were expected. That means that while the temperature of the fuel cell is rising, the polarization curves show that the current is lower.

Based on the present results, the future perspectives and challenges for further improved PEM fuel cell electrocatalysts are:

- The continuous study of different electrocatalysts in order to be established a catalogue of low and non-platinum electrocatalysts so as to be used in future experiments.
- The analysis of experimental data of different homemade MEAs' with various amounts of platinum in the anode and the cathode so as to check the stability of the PEM fuel cell that is being used.
- The scale up of the present results established by RDE measurements to single MEA experiments under typical PEM fuel cell conditions (with back pressure, humidity, 80 °C, …).
- The improving of the chemical composition stability for the catalytic pastes during voltage cycling and specifically about the bimetallic electrocatalysts.

REFERENCES

1. Stevenson, O.T.H.a.J.W. (2013) *The Role of Platinum in Proton Exchange Membrane Fuel Cells*.
2. Bagotsky, V.S., *Fuel Cells: Problems and Solutions*. 2012: Wiley.
3. Ruska, E., *The development of the electron microscope and of electron microscopy* Biosience Reports 1987 607-629.
4. Tzorbatzoglou, F., Brouzgou, A., and Tsiakaras, P., *A Review of the most efficient low-Pt and Pt-free electrocatalysts for H2 PEMFCs*, in *Fifth European Fuel Cell Technology & Applications Conference – Piero Lunghi Conference*. 2013: Rome, Italy. p. 9.
5. Rajalakshmi, N. and Dhathathreyan, K.S., *Present Trends in Fuel Cell Technology Development*. 2008: Nova Science.
6. Lucia, U., *Overview on fuel cells.* Renewable and Sustainable Energy Reviews, 2014. 30(0). 164-169.
7. Esmaeilifar, A., Rowshanzamir, S., Eikani, M.H., and Ghazanfari, E., *Preparation of low-platinum-loading electrocatalysts using electroless deposition method for proton exchange membrane fuel cell systems.* Electrochimica Acta, 2010. 56(1). 271-277.
8. Ham, D., Han, S., Pak, C., Ji, S., Jin, S.-A., Chang, H., and Lee, J., *High Electrochemical Performance and Stability of Co-Deposited Pd–Au on Phase-Pure Tungsten Carbide for Hydrogen Oxidation.* Topics in Catalysis, 2012. 55(14-15). 922-930.
9. Huggins, M.L., *THERMODYNAMIC PROPERTIES OF SOLUTIONS OF LONG-CHAIN COMPOUNDS.* Annals of the New York Academy of Sciences, 1942. 43(1). 1-32.
10. Blomen, L.M.J. and Mugerwa, M., *Epilogue*, in *Fuel Cell Systems*, L.M.J. Blomen and M. Mugerwa, Editors. 1993, Springer US. p. 583-588.
11. Ketelaar, J.A.A., *History*, in *Fuel Cell Systems*, L.M.J. Blomen and M. Mugerwa, Editors. 1993, Springer US. p. 19-35.
12. Weaver, G. and Reidy, R., *World Fuel Cells: An Industry Profile with Market Prospects to 2010*. 2002: Elsevier Advanced Technology.
13. Milewski, J., Świrski, K., Santarelli, M., and Leone, P., *Advanced Methods of Solid Oxide Fuel Cell Modeling*. 2011: Springer.

14. Okada, T. and Kaneko, M., *Molecular Catalysts for Energy Conversion*. 2008: Springer Berlin Heidelberg.
15. Cleveland, C.J. and Morris, C.G., *Handbook of Energy: Chronologies, Top Ten Lists, and Word Clouds*. 2013: Elsevier Science.
16. Behling, N.H., *Fuel Cells: Current Technology Challenges and Future Research Needs*. 2013: Elsevier.
17. Srinivasan, S., *Fuel Cells: From Fundamentals to Applications*. 2006: Springer.
18. Dreyer, W., Guhlke, C., and Landstorfer, M., *A mixture theory of electrolytes containing solvation effects.* Electrochemistry Communications, 2014. 43(0). 75-78.
19. Appleby, A.J., *FUEL CELLS – OVERVIEW | Introduction*, in *Encyclopedia of Electrochemical Power Sources*, J. Garche, Editor. 2009, Elsevier: Amsterdam. p. 277-296.
20. Cleghorn, S.J.C., Ren, X., Springer, T.E., Wilson, M.S., Zawodzinski, C., Zawodzinski, T.A., and Gottesfeld, S., *Pem fuel cells for transportation and stationary power generation applications.* International Journal of Hydrogen Energy, 1997. 22(12). 1137-1144.
21. Sammes, N., *Fuel Cell Technology: Reaching Towards Commercialization*. 2006: Springer.
22. Wallace, J.S. and Ward, C.A., *Hydrogen as a fuel.* International Journal of Hydrogen Energy, 1983. 8(4). 255-268.
23. Frumkin, A., *Über die Beeinflussung der Adsorption von Neutralmolekülen durch ein elektrisches Feld.* Zeitschrift für Physik, 1926. 35(10). 792-802.
24. Shah, R.K., *Introduction to Fuel Cells*, in *Recent Trends in Fuel Cell Science and Technology*, S. Basu, Editor. 2007, Springer New York. p. 1-9.
25. Andújar, J.M. and Segura, F., *Fuel cells: History and updating. A walk along two centuries.* Renewable and Sustainable Energy Reviews, 2009. 13(9). 2309-2322.
26. Cleveland, C.J. and Morris, C., *Section 18 - Fuel Cells*, in *Handbook of Energy*, C.J. Cleveland and C. Morris, Editors. 2014, Elsevier: Boston. p. 323-332.
27. Kordesch, K.V. and Simader, G.R., *Environmental Impact of Fuel Cell Technology.* Chemical Reviews, 1995. 95(1). 191-207.
28. Behling, N.H., *Chapter 7 - History of Proton Exchange Membrane Fuel Cells and Direct Methanol Fuel Cells*, in *Fuel Cells*, N.H. Behling, Editor. 2013, Elsevier. p. 423-600.

29. Zhang, J., *PEM Fuel Cell Electrocatalysts and Catalyst Layers: Fundamentals and Applications*. 2008: Springer.
30. Wilkinson, D.P., Zhang, J., Hui, R., Fergus, J., and Li, X., *Proton Exchange Membrane Fuel Cells: Materials Properties and Performance*. 2009: CRC Press.
31. Bouwmeester, H.J.M. and Burggraaf, A.J., *The CRC Handbook of Solid State Electrochemistry*. 1997, Nature Publishing Group. p. 481-553.
32. D. Myers, X.W., N. Kariuki, S. Niyogi, J. Mawdsley and J. D. Carter *Non-Platinum Bimetallic Cathode Electrocatalysts*, in *DOE Hydrogen Program Review*. 2008.
33. Gasteiger, H.A., Kocha, S.S., Sompalli, B., and Wagner, F.T., *Activity benchmarks and requirements for Pt, Pt-alloy, and non-Pt oxygen reduction catalysts for PEMFCs.* Applied Catalysis B: Environmental, 2005. 56(1-2 SPEC. ISS.). 9-35.
34. *Platinum and its use*. 2010; Available from: **http://www.keytometals.com/page.aspx?ID=CheckArticle&site=ktn&NM=237**.
35. Lee, K.-S. and Kim, D.M., *Sputtering and heat treatment of pure Ni metal onto a carbon nanotube on carbon paper to fabricate electrocatalysts for the oxygen reduction reaction in PEMFC.* International Journal of Hydrogen Energy, 2012. 37(7). 6272-6276.
36. Wang, M., Woo, K.-D., and Kim, D.-K., *Preparation of Pt nanoparticles on carbon nanotubes by hydrothermal method.* Energy Conversion and Management, 2006. 47(18–19). 3235-3240.
37. Shui, J.-l., Chen, C., and Li, J.C.M., *Evolution of Nanoporous Pt–Fe Alloy Nanowires by Dealloying and their Catalytic Property for Oxygen Reduction Reaction.* Advanced Functional Materials, 2011. 21(17). 3357-3362.
38. Vajtai, R., *Springer Handbook of Nanomaterials*. 2013: Springer.
39. M. Mougenot, A.C., M. Simoes, S. Baranton, C. Coutanceau, P. Brault, *PdAu/C catalysts prepared by plasma sputtering for the electro - oxidation of glycerol* 2011.
40. Matthew Brodt, R.W.a.P.N.P., *Nanofiber Electrodes with Low Platinum Loading for High Power Hydrogen/Air PEM Fuel Cells.* The Electrochemical Society, 2013. 160(8). F744-F749.
41. Cho, Y.-H., Choi, B., Cho, Y.-H., Park, H.-S., and Sung, Y.-E., *Pd-based PdPt(19:1)/C electrocatalyst as an electrode in PEM fuel cell.* Electrochemistry Communications, 2007. 9(3). 378-381.

42. Saha, M.S., Gullá, A.F., Allen, R.J., and Mukerjee, S., *High performance polymer electrolyte fuel cells with ultra-low Pt loading electrodes prepared by dual ion-beam assisted deposition.* Electrochimica Acta, 2006. 51(22). 4680-4692.

43. Antolini E, Z.S., Santos SF, Gonzalez ER., *Palladium-based electrodes: A way to reduce platinum content in polymer electrolyte membrane fuel cells.* Electrochimica Acta, 2011. 56. 2299-2305.

44. Xiong, L. and Manthiram, A., *High performance membrane-electrode assemblies with ultra-low Pt loading for proton exchange membrane fuel cells.* Electrochimica Acta, 2005. 50(16–17). 3200-3204.

45. Cavarroc, M., Ennadjaoui, A., Mougenot, M., Brault, P., Escalier, R., Tessier, Y., Durand, J., Roualdès, S., Sauvage, T., and Coutanceau, C., *Performance of plasma sputtered fuel cell electrodes with ultra-low Pt loadings.* Electrochemistry Communications, 2009. 11(4). 859-861.

46. Gruber, D., Ponath, N., Müller, J., and Lindstaedt, F., *Sputter-deposited ultra-low catalyst loadings for PEM fuel cells.* Journal of Power Sources, 2005. 150(0). 67-72.

47. Zeis, R., Mathur, A., Fritz, G., Lee, J., and Erlebacher, J., *Platinum-plated nanoporous gold: An efficient, low Pt loading electrocatalyst for PEM fuel cells.* Journal of Power Sources, 2007. 165(1). 65-72.

48. Li, B., Qiao, J., Yang, D., Zheng, J., Ma, J., Zhang, J., and Wang, H., *Synthesis of a highly active carbon-supported Ir–V/C catalyst for the hydrogen oxidation reaction in PEMFC.* Electrochimica Acta, 2009. 54(24). 5614-5620.

49. Ham, D.J., Pak, C., Bae, G.H., Han, S., Kwon, K., Jin, S.-A., Chang, H., Choi, S.H., and Lee, J.S., *Palladium-nickel alloys loaded on tungsten carbide as platinum-free anode electrocatalysts for polymer electrolyte membrane fuel cells.* Chemical Communications, 2011. 47(20). 5792-5794.

50. Marceta Kaninski, M.P., Nikolic, V.M., Tasic, G.S., and Rakocevic, Z.L., *Electrocatalytic activation of Ni electrode for hydrogen production by electrodeposition of Co and V species.* International Journal of Hydrogen Energy, 2009. 34(2). 703-709.

51. Zhang H, V.-G.Y., Jacobson AJ, Ramirez A, Chianelli RR (2003) *Transition Metal Sulfide Electrocatalysts for PEM Fuel Cells*.

52. Nallathambi, V., Lee, J.-W., Kumaraguru, S.P., Wu, G., and Popov, B.N., *Development of high performance carbon composite catalyst for oxygen reduction*

reaction in PEM Proton Exchange Membrane fuel cells. Journal of Power Sources, 2008. 183(1). 34-42.

53. Tang, J.M., Jensen, K., Waje, M., Li, W., Larsen, P., Pauley, K., Chen, Z., Ramesh, P., Itkis, M.E., Yan, Y., and Haddon, R.C., *High Performance Hydrogen Fuel Cells with Ultralow Pt Loading Carbon Nanotube Thin Film Catalysts†.* The Journal of Physical Chemistry C, 2007. 111(48). 17901-17904.
54. Li, B. and Chan, S.H., *PtFeNi tri-metallic alloy nanoparticles as electrocatalyst for oxygen reduction reaction in proton exchange membrane fuel cells with ultra-low Pt loading.* International Journal of Hydrogen Energy, 2013. 38(8). 3338-3345.
55. Hirsch, P.B., *Electron Microscopy in Material Science*. 1971. 3-11.
56. Norton, C.S.a.M.G., *'X-Ray Diffraction: A Practical Approach'*. 1988, New York.
57. Bard, A.J. and Faulkner, L.R., *Electrochemical methods: fundamentals and applications*. 1980: Wiley. 86-90.
58. Qi, Z., *Electrochemical Methods for Catalyst Activity Evaluation*, in *PEM Fuel Cell Electrocatalysts and Catalyst Layers*, J. Zhang, Editor. 2008, Springer London. p. 547-607.
59. Biotechnology, U.o.C.D.o.C.E.a. *Hydrodynamic Voltammetry*. 2013; Available from **http://www.ceb.cam.ac.uk/research/groups/rg-eme/teaching-notes/hydrodynamic-voltammetry**.
60. Tzorbatzoglou, F., Brouzgou, A., and Tsiakaras, P., *Electrocatalytic activity of Vulcan-XC-72 supported Pd, Rh and PdxRhy toward HOR and ORR.* Applied Catalysis B: Environmental, 2015, 174–175, 203-211.
61. Tzorbatzoglou, F., *Design and development of a fuel cell system (PEM type) – Water electrolysis type PEM: Preparation and characterization of low cost electrocatalysts*, PhD Thesis, March 2015, *Department of Mechanical Engineering*, University of Thessaly, Volos-Greece.
62. Wang, K., Pan, Z., Tzorbatzoglou, F., Zhang, Y., Wang, Y., Panagiotis, T., and Song, S., *An investigation of WC stability during the preparation of Pt@WC/OMC via a pulse microwave assisted polyol method.* Applied Catalysis B: Environmental, 2015. 166–167(0). 224-230.